Magnetite microexsolutions in silicate and magmatic flow fabric of the Goyozan granitoid (NE Japan): Significance of partial remanence anisotropy

Magnetite microexsolutions in silicate and magmatic flow fabric of the Goyozan granitoid (NE Japan): Significance of partial remanence anisotropy

Yoichi Usui,[1] Norihiro Nakamura,[1] and Takeyoshi Yoshida[1]

Received 25 November 2005; revised 23 May 2006; accepted 8 June 2006; published 8 November 2006.

[1] Anisotropy of magnetic susceptibility (AMS) has been widely used to infer magmatic flow patterns of granitoids where an appropriate AMS axis is parallel to an alignment of mafic minerals or magnetite. The magmatic flow fabric in Cretaceous granitic plutons from northeastern Japan was verified using an analysis of anisotropy of partial anhysteretic remanent magnetization (ApARM) which further isolates the magnetite subfabrics according to magnetite grain size. The preferred orientation of polysynthetic twins in plagioclase laths and clinopyroxene is discordant with the bulk AMS fabric along outer marginal zones of the granitoid, as shown by image analysis of microphotographs from thin sections cut in orthogonal planes. This suggests that the uncorroborated use of bulk AMS to detect flow fabric in granitoids has risks. Scanning electron microscopy (SEM) reveals that submicroscopic, needle-shaped magnetite inclusions exsolved in anhedral plagioclase and clinopyroxene may explain such anomalous exceptions to the validity of AMS fabrics. Our ApARM measurements show that the ApARM alignment of relatively high-coercive, submicroscopic magnetite inclusions is concordant to the linear orientation of anhedral plagioclase and clinopyroxene. The combination of SEM, AMS, and ApARM was required to confirm the magmatic and submagmatic flow pattern of granitoids in this study and is generally preferable to the use of AMS alone.

Citation: Usui, Y., N. Nakamura, and T. Yoshida (2006), Magnetite microexsolutions in silicate and magmatic flow fabric of the Goyozan granitoid (NE Japan): Significance of partial remanence anisotropy, *J. Geophys. Res.*, *111*, B11101, doi:10.1029/2005JB004183.

1. Introduction

[2] The generation and emplacement of granitoids are fundamental processes in the evolution of continental crust. Magmatic flow patterns of granitoids may reveal penetrative planar and linear petrofabrics due to magmatic flow, submagmatic flow or high-temperature solid-state flow [e.g., *Paterson et al.*, 1989; *Lejeune and Richet*, 1995; *Bouchez et al.*, 1997; *Picher*, 1997]. The anisotropy of magnetic susceptibility (AMS) is now widely used to infer the petrofabrics of both paramagnetic and ferromagnetic granitoids for detecting feeder centers and exploring geodynamic significance in granitic complex [e.g., *Ellwood and Whitney*, 1980; *Bouchez et al.*, 1990; *McNulty et al.*, 2000]. It is commonly assumed that AMS foliation and lineation are parallel to the mean penetrative planar and linear petrofabrics, and hence define flow axes [*Heller*, 1973; *Tarling and Hrouda*, 1993; *Cruden and Launeau*, 1994; *Archanjo et al.*, 1995; *Launeau and Cruden*, 1998; *Pignotta and Benn*, 1999]. However, in this study, we find large discrepancies between AMS and the orientation of framework-forming silicates of plagioclase/clinopyroxene laths. The latter formed early in the crystallization history, marking the magmatic and submagmatic flow direction of granites. Moreover, recent AMS and image analysis studies of some basaltic dike swarms have also found large discrepancies between the magnetic lineation and plagioclase linear fabric [*Archanjo et al.*, 2002; *Geoffroy et al.*, 2002; *Archanjo and Launeau*, 2004]. We will show that the anisotropy of partial anhysteretic remanent magnetization (ApARM) may resolve these difficulties.

[3] AMS in granitoid combines petrofabric contributions dominantly from magnetite (mostly multidomain) as well as mafic silicates, but negligibly from framework-forming silicates of plagioclase, pyroxene, and feldspar. Because such framework-forming silicates usually have low magnetic susceptibilities, an investigation of the relationship between the framework-forming silicates and magnetic fabrics is recommended when AMS is used for mapping magmatic flow patterns in granitoids [*Launeau and Cruden*, 1998]. Normally, AMS fabrics (lineation and foliation) are parallel to the magmatic flow, submagmatic flow or high-temperature solid-state fabric defined by the elongate mafic xenoliths and by the preferential alignment of inequant magnetite [*Hrouda*, 1982; *Benn et al.*, 1993; *Archanjo et al.*, 1995; *Borradaile and Henry*, 1997]. This parallelism indicates that the magnetite and mafic minerals grew along the edges of preferentially oriented silicate laths after

[1]Department of Earth Sciences, Tohoku University, Sendai, Japan.

0148-0227/06/2005JB004183$09.00

magma flow ceased [*Hargraves et al.*, 1991]. Although AMS of ferromagnetic granitoids is generally controlled by the shape-preferred orientation of interstitial magnetites, *Borradaile and Kehlenbeck* [1996] reported the discrepancy that K-feldspar megacrysts aligned concentrically with pluton margins, whereas AMS fabrics were planar and cut across the intrusions. They attributed this discrepancy to a superimposed ''cryptic tectonic'' magnetic fabric due to posttectonic stress alignment of intragranular domain walls in multidomain magnetites. Moreover, some AMS and image analysis studies in granitoids indicate that the fabrics of plagioclase are noncoaxial to AMS principal orientation, although they attributed the noncoaxiality to the flow-induced local inversion of magnetite and mafic minerals before crystallization of magma is complete [*Cruden et al.*, 1999] or to the two-stage acquisition of magmatic fabric [*Pignotta and Benn*, 1999]. Therefore the posttectonic or syntectonic overprinting of AMS fabric appears to mask the fabric of low-susceptibility silicates, and thus the AMS fabric does not proxy for magmatic and submagmatic flow.

[4] Plagioclase orientation is commonly a good proxy for magmatic flow direction during the emplacement of granitoids because its long axis preferentially aligns with the flow line. Bulk petrofabrics of framework-forming silicates determined by the intercept counting method [*Saltikov*, 1958] have provided essential information on magmatic flow pattern in granitic plutons [e.g., *Launeau and Robin*, 1996]. To determine the plagioclase orientation, the intercept method has often been used to infer the boundary orientations of plagioclase by multispectral classification and the two dimensional orientation of plagioclase fabric is given by the long axis of a petrofabric ellipse [*Launeau and Cruden*, 1998]. Although this method effectively determines the grain boundary fabric, a thin section method shows only a small area of a rock that may not represent the typical fabric at an outcrop [*Borradaile*, 2003; *Borradaile and Jackson*, 2004]. An AMS measurement integrates the orientation distribution over a volume of 10.5 cm^3, encompassing at least hundreds of ferromagnetic and paramagnetic minerals. However, the AMS contribution of high-susceptibility trace minerals may mask the subfabric of low-susceptibility silicates, such as plagioclase. Therefore the study of plagioclase fabric resulting from magmatic flow requires the separation of the low-susceptibility silicate fabric component from the bulk (i.e., combined ferromagnetic and paramagnetic) AMS fabric.

[5] Acquisition of anhysteretic remanent magnetization (ARM) is hindered by coercivity of remanence [*Jackson*, 1991]. Coercivity of remanence (H_{cr}) is related to and exceeds the coercive force H_c. For magnetite (magnetically soft mineral), the coercive force can be related to grain size (d) by a power law function as $H_c \sim d^{-n}$, where n varies from 0 to 1 [*Day et al.*, 1977; *Dunlop and Özdemir*, 1997]. When intragranular domain walls are pinned by ordered arrays of defects or dislocations, the power index corresponds to $n = 0.5$ [*Stacey and Wise*, 1967], which agrees with the natural occurrence of $n = 0.4–0.6$ in magnetite above the critical single-domain size [*Dunlop and Özdemir*, 1997]. Using the power law function, *Jackson et al.* [1988] first showed the principle of isolating different orientation of distributions of different magnetite subfabrics by employing different coercive force windows for the same sample. Recent ApARM studies have focused on only two coercive force windows for ''coarse-grained'' euhedral magnetite and ''fine-grained'' secondary magnetite [*Trindade et al.*, 1999; *Bolle et al.*, 2003; *Diot et al.*, 2003; *Giroux and Benn*, 2005]. However, magnetite is defined by three distinct types of domain wall structures of multidomain (MD), pseudosingle-domain (PSD) and single-domain (SD), each of which is associated with a restricted size range, assuming dislocation densities and chemical composition effects may be disregarded. The latter two assumptions are valid in our study since the granitoids are magnetite series and the magnetite is essentially ''stress free.'' Because the AF windows required to isolate these grain sizes vary from one rock type to another, we employ the most useful coercivity windows revealed by a pilot study in our samples: (1) 0–3 mT for coarse-grained magnetite; (2) 3–15 mT for medium-grained magnetite, and (3) 15–60 mT for fine-grained magnetite (as by *Nakamura and Borradaile* [2001]). These coercive force windows isolate the partial orientation distribution of various sizes of natural magnetites in our granitic plutons; other plutons may require different AF windows. ApARM ellipsoids for each coercive force window and AMS ellipsoid ($k_1 \geq k_2 \geq k_3$) were determined from the body-diagonal seven-orientation scheme of *Borradaile and Stupavsky* [1995]. It may also be noted that in some situations the statistical treatment of AMS data alone may permit the discrimination of two subfabrics, for example, by comparing normalized and nonnormalized mean tensors or comparing subfabrics characterized by different bulk susceptibility [*Borradaile and Gauthier*, 2001; *Borradaile*, 2003; *Borradaile and Gauthier*, 2003].

[6] Recent ApARM studies on granitoids have revealed well-defined oblique fabrics between AMS and fine-grained ApARM and attributed such obliquity to be interpreted as evidence in granitoids for secondary geological processes such as hydrothermal alteration to cause the mineralization of fine-grained magnetites in microfractures [*Trindade et al.*, 1999; *Bolle et al.*, 2003]. However, not all the fine-grained ApARM fabric is secondary in origin. *Xu et al.* [1997], *Renne et al.* [2002], and *Feinberg et al.* [2004] have claimed that submicroscopic magnetite inclusions exsolved in plagioclase and clinopyroxene are good candidates for paleomagnetic studies because of their high-coercivity and high-temperature origin. Therefore the fine-grained magnetite inclusions may proxy as preferred orientations for their plagioclase host crystals. The orientation of fine-grained or medium-grained magnetite inclusions hosted in silicates may be discriminated by ApARM, whereas a ApARM fabric for accessory coarse-grained magnetite may correspond to the bulk AMS fabric [*Borradaile*, 1994; *Borradaile and Jackson*, 2004]. In this paper, we present results of a detailed AMS and ApARM study of the Goyozan granitic pluton, a typical Mesozoic intrusion of arc magmatism in northeastern Japan. The scanning electron microscopy (SEM) shows that exsolved magnetite inclusions within plagioclase and clinopyroxene are the chief contributors to ApARM and suggests that ApARM in granitoids is a direct reflection of magnetically less detectable plagioclase

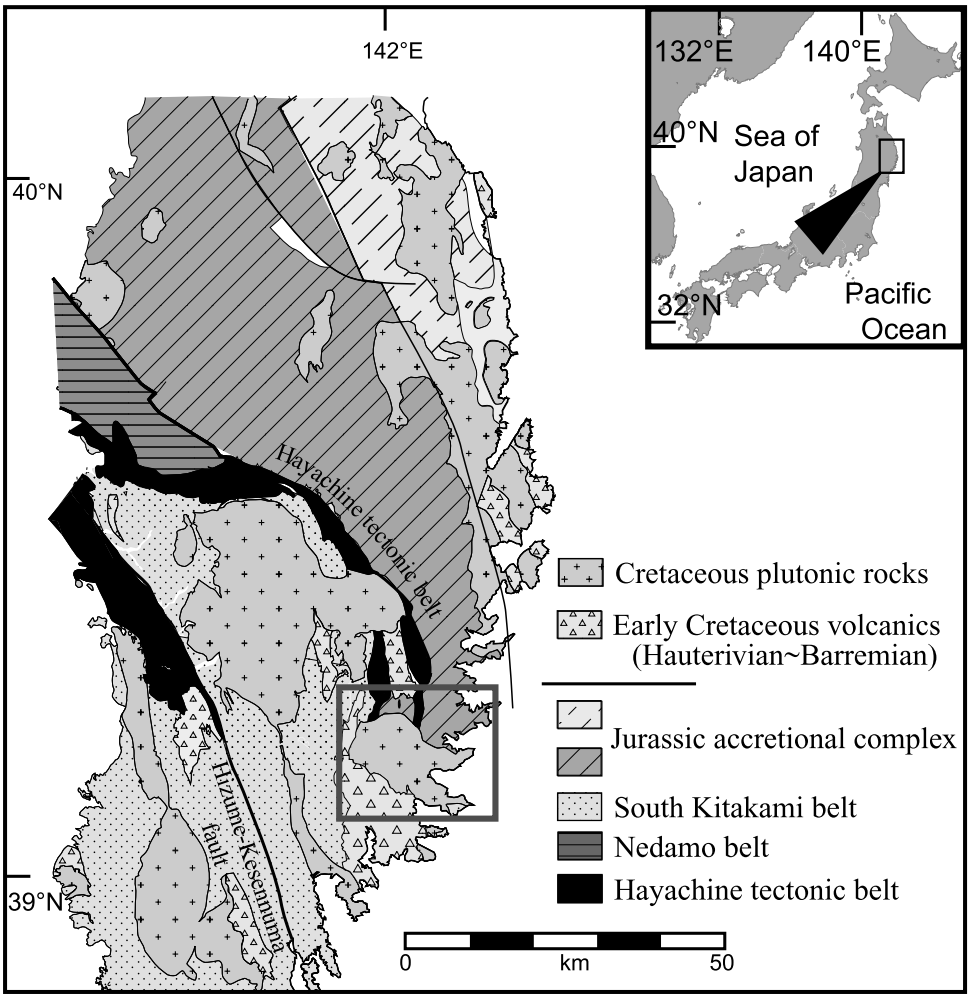

Figure 1. Geological map of northeastern Japan, showing the location of the Goyozan plutonic complex.

fabric, which is formed early in the crystallization history and best defines flow.

2. Geological Background

[7] Early Cretaceous plutonic rocks in the northeastern Japan arc were formed by intrusion of silicic plutons into Paleozoic and Mesozoic sedimentary and volcanic rocks in response to the westward subduction of the oceanic Pacific plate beneath eastern Eurasia [*Engebretson et al.*, 1985; *Otsuki*, 1992] (Figure 1). The plutons represent the roots of a magmatic arc related to the westward subduction of the Izanagi plate [*Maruyama and Seno*, 1986] along the eastern margin of the East Asian continent. The Goyozan plutonic complex is one of the early Cretaceous plutons in northeastern part of the Japan arc. It emplaced across the Hayachine tectonic belt which separates the north Kitakami belt of Jurassic accretional complex from the south Kitakami belt of pre-Silurian basements [*Ehiro and Kanisawa*, 1999; *Ehiro and Suzuki*, 2003]. The tectonic belt is defined as two fault zones comprising basic to ultrabasic rocks of an Ordovician arc ophiolite [*Shibata and Ozawa*, 1992]. The Ordovician arc ophiolite has been separated by the Hizume-Kesennuma fault, being displaced to the south in the early Cretaceous by a sinistral strike-slip fault [*Ehiro*, 1977; *Ozawa*, 1984]. The complex includes granitoid over an area of 175 km^2, 107–128 Ma (early Aptian) in K-Ar age [*Kawano and Ueda*, 1966], and intrudes into early Cretaceous andesitic volcanics of the Ohfunato Group (Hauterivian–Barremian) and Paleozoic-Mesozoic basement rocks of the north and the south Kitakami belts. The granitoid comprises three subplutons: Yoshihama-type, Okuboyama-type, and Kuroiwa-type [*Kajitani*, 1977; *Nishioka and Yoshioka*, 2004; *Takeuchi et al.*, 2005] (Figure 2). The Yoshihama type is a medium-grained clinopyroxene bearing biotite–hornblende granodiorite–hornblende–biotite tonalite, which is distributed throughout most parts of the area. The Okuboyama type is a fine to medium-grained hornblende-biotite tonalite, which intrudes into the Yoshihama type in the central part of the area with the presence of chilled margins. Finally, the Kuroiwa type is a medium-grained hornblende-biotite granodiorite, which intrudes into the Yoshihama type in the northwestern part of the area.

[8] Most outcrops show weak or negligible foliations defined by a preferred orientation of hornblende and biotite. No lineation is discernible in the field. The foliation strikes N-S to NNW-SSE and dips steeply in the western and central part of the granitoid, which appears to be developed

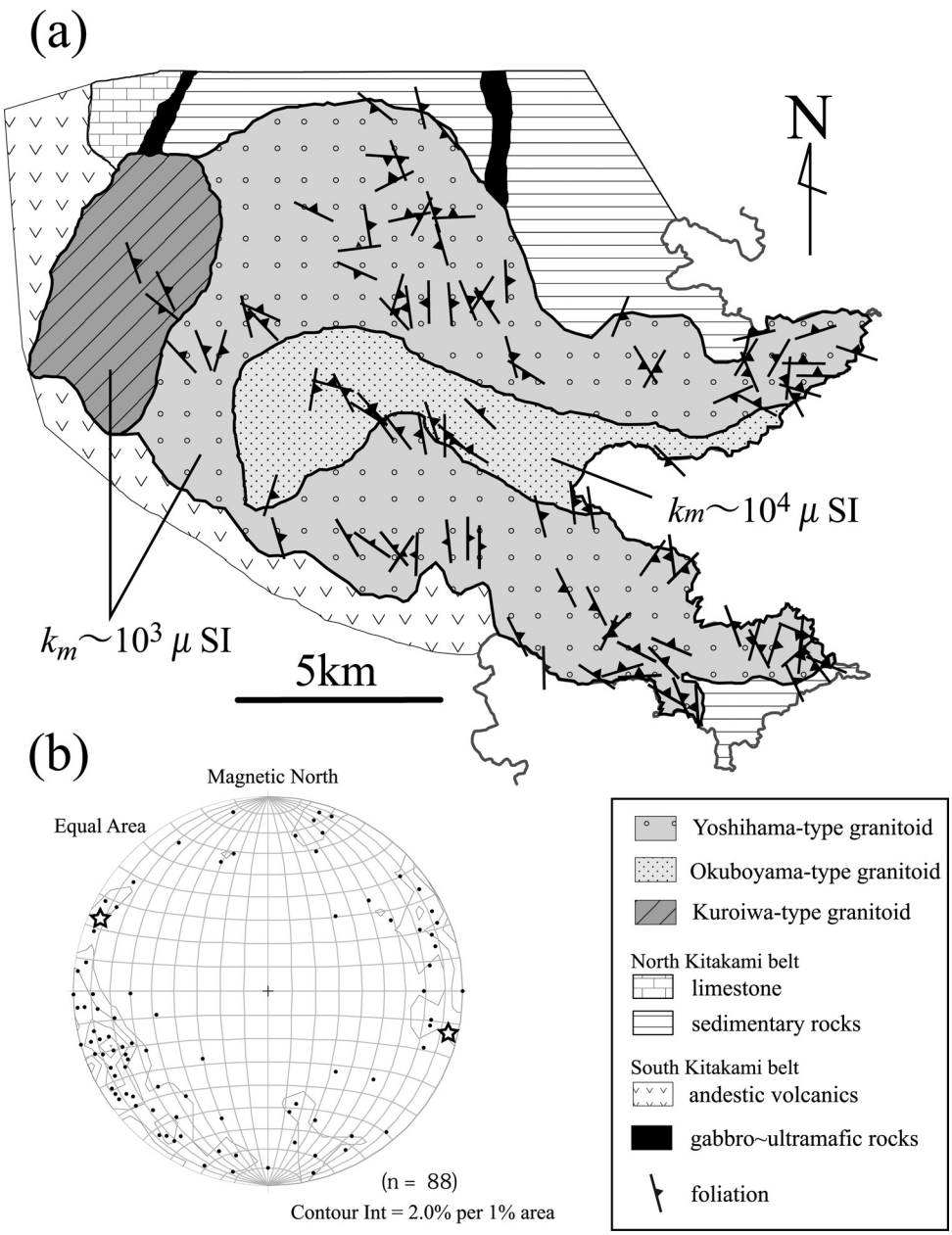

Figure 2. Internal structures and a geological sketch of the Goyozan plutonic complex and surrounding areas. The complex comprises three subplutons: Yoshihama type (bulk magnetic susceptibility, $k_m \sim 10^3$ μSI), Okuboyama type ($k_m \sim 10^4$ μSI), and Kuroiwa type ($k_m \sim 10^3$ μSI). (a) Visible foliation planes defined by mafic mineral alignments of hornblende and biotite. N-S to NNW-SSE striking foliations are dominant in the western and central part of the granitoid, while WNW-ESE to E-W striking foliations are distributed in the whole area of the granitoid, even within the central part. (b) Density contours of poles to mineral foliation planes defined by field surveys (data from this study and S. Seto, unpublished data, 1997). Stars are poles to orientations of two ultramafic rocks in the northern area, not being consistent with mineral foliations.

under a westward subduction-induced transpressional plate tectonic setting (Figure 2a). The foliation planes of mafic minerals are oblique to the traces of the granitoid walls. The foliation strikes WNW-ESE to E-W with moderate dips in the eastern part. Figure 2b shows foliation pole data of preferred orientations of mafic minerals on lower hemisphere Schmidt projections (StereoWin v.1.1 by R. Allmendinger) with orientations of the Hayachine tectonic belt, being oblique to the foliation trend. Previous gravity survey of the Goyozan plutonic complex revealed low anomaly zones, centered on the north central part of the Yoshihama-type granitoid (Figure 3a), being higher outward toward the southeastern margins [*Nabetani and Kano*, 1977; *Kano*, 1978; *Nabetani*, 1982; *Komazawa et al.*, 1996]. A model gravity profile using Chebyshev polynomials approximation method showed that the bulk of the pluton is tabular and

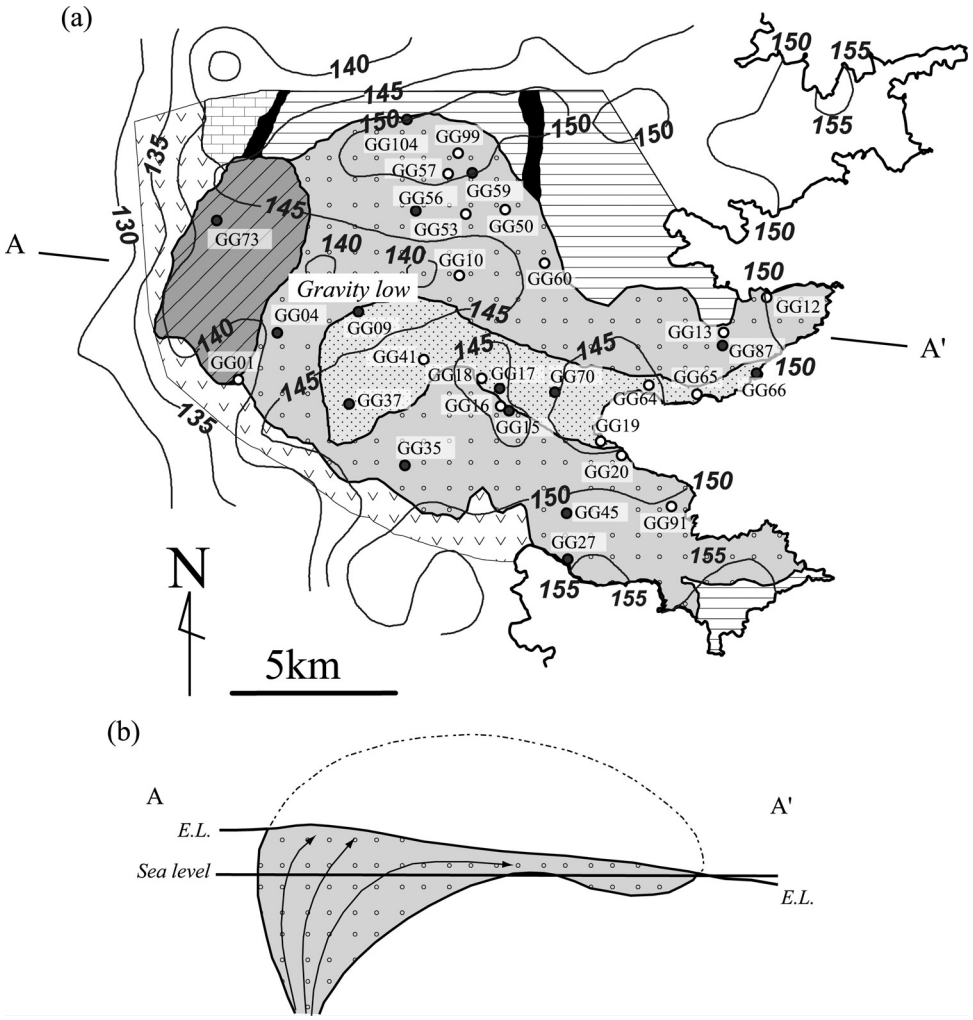

Figure 3. Gravity map with sampling locality and an emplacement model of the Goyozan plutonic complex (traced from *Komazawa et al.* [1996]). (a) Bouguer gravity anomaly map (in mGal) of the complex and surrounding areas. Localities of 36 AMS sampling stations are shown by circles. Solid circles indicate the 15 stations with ApARM fabric measurements. (b) Modeled A-A′ cross section at present elevation level (E.L.) of the Goyozan plutonic complex. Model gravity profile and structural foliation pattern suggest that granitic magma was fed by a vertical conduit centered on north central part of the Yoshihama type and that magma spread laterally to the SE and east to form the tabular pluton [after *Kano*, 1978].

<3 km thick with a deeper (~7–9 km) root on its north side [*Kano*, 1978; *Nabetani*, 1982] (Figure 3b). Examination of the structural pattern in combination with the gravity data suggests that granitic magma was fed by a vertical conduit centered on the north central part of the Yoshihama-type granitoid and that magma spread laterally to the SE and east to occupy the bulk of the body [*Kano*, 1978]. Inside the granitoid, sampling was conducted at 41 stations: 27 stations in the Yoshihama type, 13 stations in the Okuboyama type, and 1 station in the Kuroiwa type (Figure 3a). At each station, we collected one oriented hand specimen. In the laboratory, four to nine cylindrical core samples (2.2 cm in length and 2.5 cm in diameter) for magnetic measurements were drilled from each hand specimen, using a diamond-tipped drill bit and nonmagnetic diamond saw blade. We acquired a total of 297 cylindrical core samples.

[9] The main rock-forming minerals of the granitoid are plagioclase, orthoclase, quartz, hornblende and biotite, opaque phases (mainly magnetite) and apatite and zircon as accessory minerals (Figures 4a–4c). Plagioclase grains show euhedral shapes and retain a dimensional preferred elongation where albite or Carlsbad twin interfaces are parallel to the direction of elongation. Most euhedral magnetites of more than 3 μm in size (coarse-grained magnetite) are sparsely observed as free accessory opaques under the optical microscope (Figures 4a–4c). Clots of coarse-grained and medium-grained magnetites (smaller than 3 μm in size) are observable along cleavages and margins of biotite and hornblende (Figure 4d). Clinopyroxene is commonly included in the core of hornblende, only observed in the outer marginal zone of the Yoshihama-type granitoid (Figure 4e). Much finer grained magnetites are present as microexsolutions in clinopyroxene and plagioclase (Figures 4e and 4f). Hornblende and biotite are more abundant in the Yoshihama-type and the Kuroiwa-type intrusions (i.e., granodioritic) than in the Okuboyama type (tonalite). On the other hand, mag-

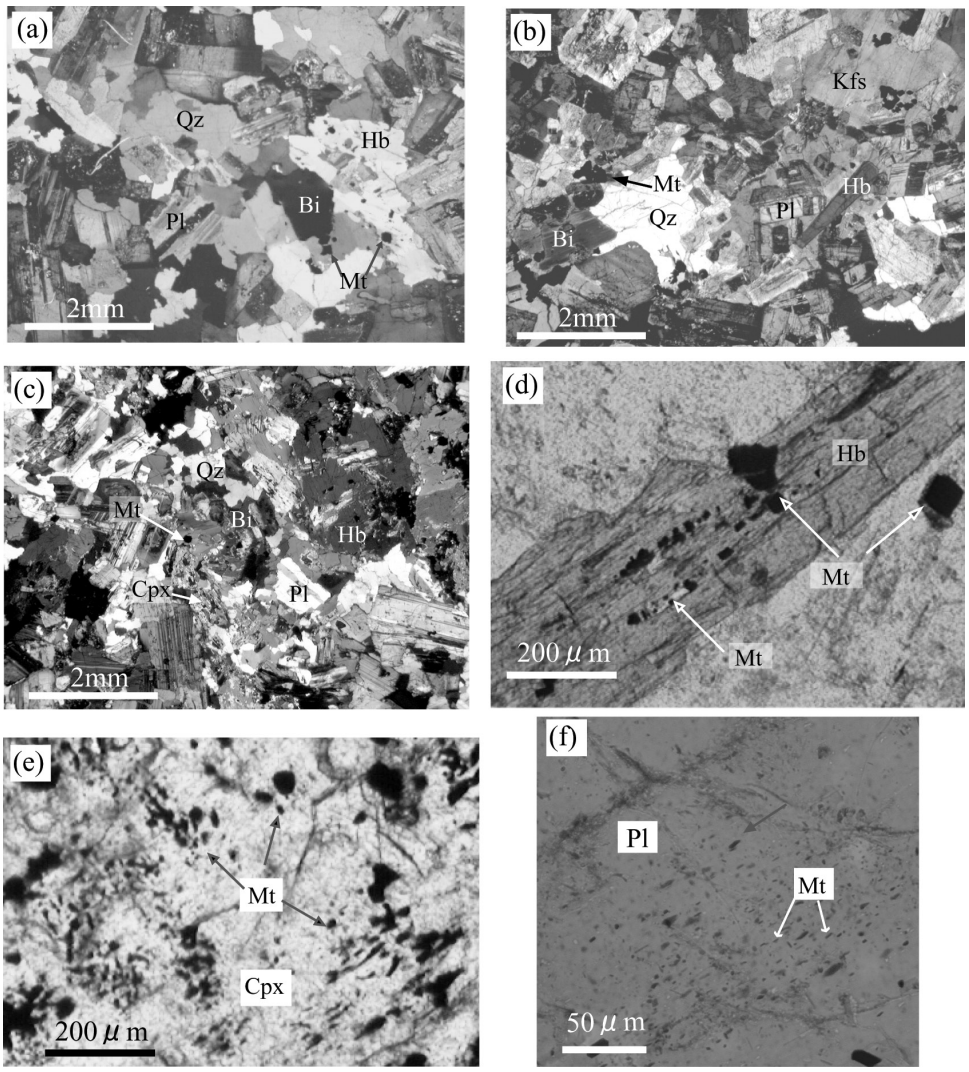

Figure 4. Photomicrographs (transmitted light) of thin sections from the Goyozan granitoid. (a) Overview of fabric of the Yoshihama-type (tonalite) intrusion in crossed polars. Plagioclase grains show euhedral shapes and retains a dimensional preferred elongation where albite or Carlsbad twin interfaces are parallel to the direction of elongation. (b) Overview of fabric of the Okuboyama-type (tonalite) intrusion in crossed polars, being more felsic and ferromagnetic than the Yoshihama type. (c) Clinopyroxene-bearing Yoshihama-type granitoid, being commonly included in the core of hornblende, only observed in the outer marginal zone of the Yoshihama-type, crossed polars. (d) Euhedral coarse-grained magnetites and clots of medium-grained magnetites in the hornblende host, uncrossed polars. (e) Oxide microexsolutions in clinopyroxene, uncrossed polars. (f) Oxide microexsolutions in plagioclase, uncrossed polars. Qz, quartz; Pl, plagioclase; Kfs, potassium feldspar; Hb, hornblende; Bi, biotite; Cpx, clinopyroxene; Mt, magnetite.

netite is more abundant in the Okuboyama type than two other rock types (Figures 4a and 4b). The lack of significant crystallographic deformation features (e.g., quartz subgrain, undulation or microfractures) in thin sections of the majority of samples from the granitoid (Figures 4a, 4b, and 4c) indicates that the foliation was acquired by magmatic and submagmatic flow alignment before complete crystallization [*Paterson et al.*, 1989].

3. Magnetic Mineralogy

[10] Interpretation of AMS and ApARM requires a determination of which minerals contribute to induced and which contribute to remanent magnetization. Before measuring anisotropic magnetic fabrics, magnetic mineralogy was investigated in samples from each subpluton through optical microscopy, bulk (induced) magnetic susceptibility and coercivity spectra [*Jackson et al.*, 1988]. Optical microscopy indicates that paramagnetic minerals in the Goyozan granitoid are biotite, hornblende and clinopyroxene. Opaque mineralogy is dominated by ubiquitous euhedral coarse-grained and medium-grained magnetite (Figure 4d). Mostly their intergrain distances exceed the average grain size, suggesting that magnetic interactions are not significant [*Fuller*, 1963; *Hargraves et al.*, 1991; *Grégoire et al.*, 1995; *Cañón-Tapia et al.*, 1996]. Clino-

Table 1. AMS Data

Site	Rock Type	Number of Core	Dec/Inc			Site Mean Magnetic Foliation		k_m, 10^{-6} SI	P_j	T_j
			Site Mean k_1 (max)	Site Mean k_2 (int)	Site Mean k_3 (min)	Strike	Dip			
1	Yoshihama	4	277/46	184/3	91/44	1	46	7,128	1.19	−0.24
4	Yoshihama	9	151/5	339/85	241/0	151	90	13,890	1.08	0.08
10	Yoshihama	8	346/65	160/25	251/2	161	88	5,552	1.10	0.27
12	Yoshihama	6	96/75	244/13	335/8	245	82	73	1.02	0.48
13	Yoshihama	7	159/82	2/13	298/6	208	84	2,926	1.03	−0.19
14	Yoshihama	9	5/67	269/3	178/22	88	68	3,074	1.11	−0.12
15	Yoshihama	6	142/52	337/37	241/8	151	82	6,481	1.15	0.12
16	Yoshihama	6	142/49	347/38	247/13	157	77	8,301	1.10	0.52
20	Yoshihama	7	147/2	247/80	56/10	326	80	5,620	1.06	−0.14
27	Yoshihama	7	114/59	2/13	265/28	175	62	10,290	1.16	−0.09
35	Yoshihama	5	67/71	329/3	238/19	148	71	10,770	1.16	−0.26
45	Yoshihama	6	173/62	269/3	1/28	271	63	3,653	1.16	−0.41
46	Yoshihama	8	12/64	179/26	271/5	181	85	4,877	1.15	−0.72
50	Yoshihama	8	216/86	23/4	113/1	23	89	1,850	1.07	−0.33
53	Yoshihama	9	5/70	177/19	268/3	178	87	5,668	1.07	−0.13
54	Yoshihama	9	300/49	187/19	83/35	353	55	3,436	1.07	−0.03
55	Yoshihama	8	1/53	154/34	253/13	163	77	5,050	1.06	−0.18
56	Yoshihama	8	146/81	17/6	286/7	196	83	5,925	1.04	−0.04
57	Yoshihama	7	161/85	313/5	43/3	313	87	4,767	1.05	−0.64
59	Yoshihama	6	89/84	240/5	330/3	240	87	7,123	1.08	−0.61
60	Yoshihama	7	96/65	199/6	291/24	201	66	389	1.05	0.02
87	Yoshihama	6	330/53	230/7	135/36	45	54	1,993	1.06	0.19
91	Yoshihama	7	330/60	177/28	81/12	350	78	4,062	1.08	−0.34
99	Yoshihama	6	206/76	116/0	26/14	296	76	9,110	1.10	−0.67
104	Yoshihama	6	157/64	349/25	257/5	167	85	20,220	1.17	−0.45
9	Okuboyama	13	346/75	153/15	244/3	154	87	32,710	1.14	−0.1
17	Okuboyama	9	148/44	327/46	58/0	328	90	33,170	1.08	0.29
18	Okuboyama	6	163/34	344/56	253/0	163	90	32,000	1.11	−0.2
19	Okuboyama	5	159/22	14/63	255/14	165	76	31,600	1.09	0.34
37	Okuboyama	9	357/42	165/47	261/6	171	84	26,310	1.12	0.31
41	Okuboyama	5	342/42	106/32	218/31	128	59	27,720	1.13	0.1
64	Okuboyama	6	84/47	338/13	237/40	147	50	26,710	1.04	0.15
65	Okuboyama	5	351/42	126/38	237/25	147	65	34,680	1.08	−0.51
66	Okuboyama	8	329/48	185/36	81/19	351	71	32,810	1.11	−0.31
70	Okuboyama	7	180/14	6/76	270/2	180	88	34,250	1.14	−0.08
93	Okuboyama	8	0/59	176/31	267/2	177	88	22,430	1.12	0.44
73	Kuroiwa	8	97/45	345/20	238/38	148	52	7,222	1.07	−0.07

pyroxene crystals usually contain opaque exsolutions (Figure 4e). In samples from the southern marginal zone (e.g., GG27), submicron opaque rods were observed within plagioclase crystals (Figure 4f). Oxide microfracture was not observed under the optical microscope. However, fine-grained secondary magnetite may follow cleavage surfaces or microfractures and would be difficult to observe by optical microscope as noted by *Trindade et al.* [2001]. More detailed observations by SEM are presented in a following section in this paper.

[11] Bulk magnetic susceptibility k_m was measured using a Sapphire Instrument SI2B system using an applied field of ~100 μT at 19,200 Hz (Table 1). For the Yoshihama- and the Kuroiwa-type intrusions (Figure 2), k_m varies from 500 to 20,000 (μSI), while this value ranges from 22,000 to 33,000 (μSI) for the Okuboyama type. The higher susceptibility for the Okuboyama type is consistent with the thin section observation for the higher content of coarse-grained and medium-grained magnetite (Figures 4a and 4b). Although the higher bulk susceptibility k_m indicates the strong contribution of magnetite [*Rochette*, 1987], it only partly camouflages the orientation distribution of the paramagnetic minerals.

[12] Remanent coercivity spectra were determined for five representative sampling stations from the Goyozan granitoid. The selected stations are homogeneously distributed in the pluton and their bulk susceptibilities (7100–33,000 μSI) almost cover the whole range of values found in AMS measurements. A coercivity spectrum is measured for the normalized intensities of partial ARM using a partial ARM procedure [*Jackson et al.*, 1988]. We exposed the samples to an AF peak of 150 mT at intervals of 3 mT from 0–3 up to 57–60 mT (for GG27, up to 74–77 mT) with a DC field of 0.1 mT. The coercivity spectra all exhibit a strong peak value of the pARM at low AF peak values (<30 mT), followed by a monotonically convex-down shape decrease down to the background remanent magnetization, except for GG27 (Figure 5). This shows a smooth monotonic decrease after second peak of 24–27 mT with increasing AF magnetization. Although the spectra show the monotonical decrease, optical microscopic observations reveal different size occurrences of magnetite (Figures 4d, 4e, and 4f). Compared to the other sample, the spectrum of GG27 shows higher intensity in high-coercivity region. According to magnetite coercivity versus grain size data [*Dunlop and Özdemir*, 1997], the second peak coercivity

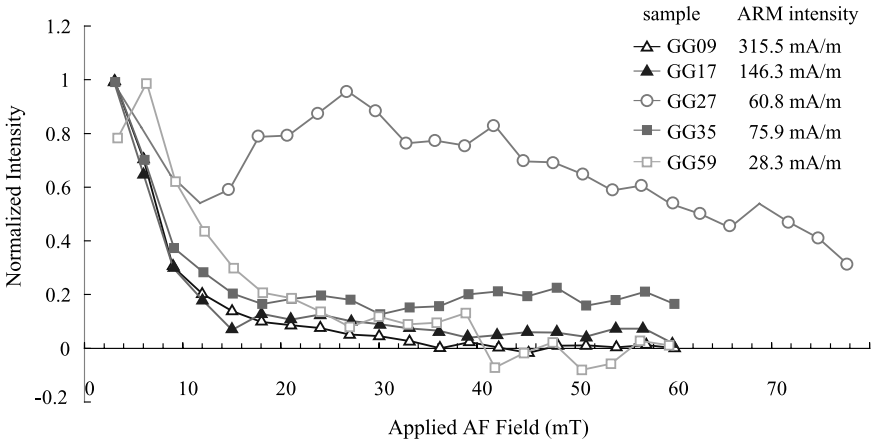

Figure 5. Maximum ARM intensity and normalized coercivity spectra of specimens from five representative stations (GG09 and GG17 from the Okuboyama type and GG27, GG35, and GG59 from the Yoshihama type). The spectra show a peak intensity <10 mT, followed by monotonic decrease except for GG27. The spectrum of GG27 shows much higher intensity in the high-coercivity part, implying a higher content of fine-grained magnetite and/or hematite.

24–27 mT corresponds to magnetite grains <0.5 μm. Thus it is implied that GG27 contains abundant high-coercive submicron magnetite and also hematite.

4. Magnetic Anisotropies

4.1. AMS

[13] AMS was measured on all of 297 cylindrical core samples (41 stations), using a Sapphire Instrument SI2B. AMS data are summarized in Table 1 and are represented as tensor mean orientations for principal axes (k_1, maximum; k_2, intermediate; k_3, minimum) with 95% confidence ellipsoids (Figures 6a and 6b). The eigenvectors within the stations are generally well grouped on lower hemisphere Schmidt projections. The AMS foliations and lineations are plotted on a map in Figure 6a. Magnetic foliations display a coherent structural pattern throughout the Goyozan pluton. The AMS fabric of the granitoid compares favorably with a preferred alignment of mafic minerals determined in the field (Figure 6b). The correlation between magnetic and structural pattern may allow us to infer magmatic flow patterns from AMS. The magnetic lineations define two distinct orientations. In the Okuboyama type, lineations are horizontal to shallow plunging and slightly oblique to the granitoid walls. In the Yoshihama type, lineations plunge steeply in the northern part, indicating a magmatic feeder zone. Previous gravity survey supports this observation (Figures 3a and 3b). In the southern margin of the Yoshihama type, the lineations also plunge steeply, implying the presence of another cryptic magmatic feeder zone. This contradicts the previous gravity survey. The shape and intensity of ellipsoids were described by Jelinek's parameter T_j (oblate to prolate; +1 to −1) and P_j (sphere to ellipsoid; 1 to ∞) (Figure 6c) [*Jelinek*, 1981].

4.2. Anisotropy of Partial Anhysteretic Remanent Magnetization

4.2.1. Methods

[14] Partial ARM is imparted to a cylindrical core sample by applying a DC field in between two chosen values of a decaying AF field [*Jackson et al.*, 1988]. To synchronize a DC field supply to an AF demagnetizer, we employ an ammeter with comparator function (Yokokawa-denki WT100) equipped with an AF demagnetizer (Natsuhara-Giken DEM95). The ammeter senses an AF coil current, and controls the interval of the constant DC field between two chosen AF fields. This direct approach is similar to the SI4 AF demagnetizer with ARM generation system of Sapphire Instruments. The DC field was 100 μT and the AC field ranges from 0 to 150 mT. Anisotropy of ARM was determined by remanence measurements along seven different axes through the specimen including body diagonal directions proposed by Nye [*Nye*, 1957; *Borradaile and Stupavsky*, 1995], using Borradaile's custom-made sample holder. This requires a special sample holder. Nye's seven-orientation scheme covers a hemisphere more uniformly than the conventional *Girdler*'s [1961] six- or nine-orientation scheme that is restricted to axes parallel to cube edges. At the same time, the seven-orientation scheme is much less time consuming than other schemes using a 12- or 18-orientation. Triaxial tumbling AF demagnetization at 150 mT was performed before imparting ApARM along each seven directions, so that a succeeding ARM is independent of any previous remanence or gyroremanent magnetization [*Stephenson*, 1981a, 1981b]. However, there is nonzero remanence after AF demagnetization at 150 mT, also called the background remanence, carried mostly by hematite.

[15] Background remanence is the residual vector that may be included in the partial ARM at each measurement step, if the specimen is unsuitably coercive or unsuccessfully demagnetized. The subtraction before calculation of ApARM tensors should be standard practice [*McCabe et al.*, 1985]. Since the Nye-7 scheme does not use self-canceling antiparallel directions [*Borradaile and Stupavsky*, 1995], the background remanence may deflect anisotropies [*Trindade et al.*, 2001]. However, the SI205 software compares each applied ARM orientation with the orientation of the applied field; if they differ the operator is alerted to the possibility of a sample that is too coercive for ApARM measurement. In

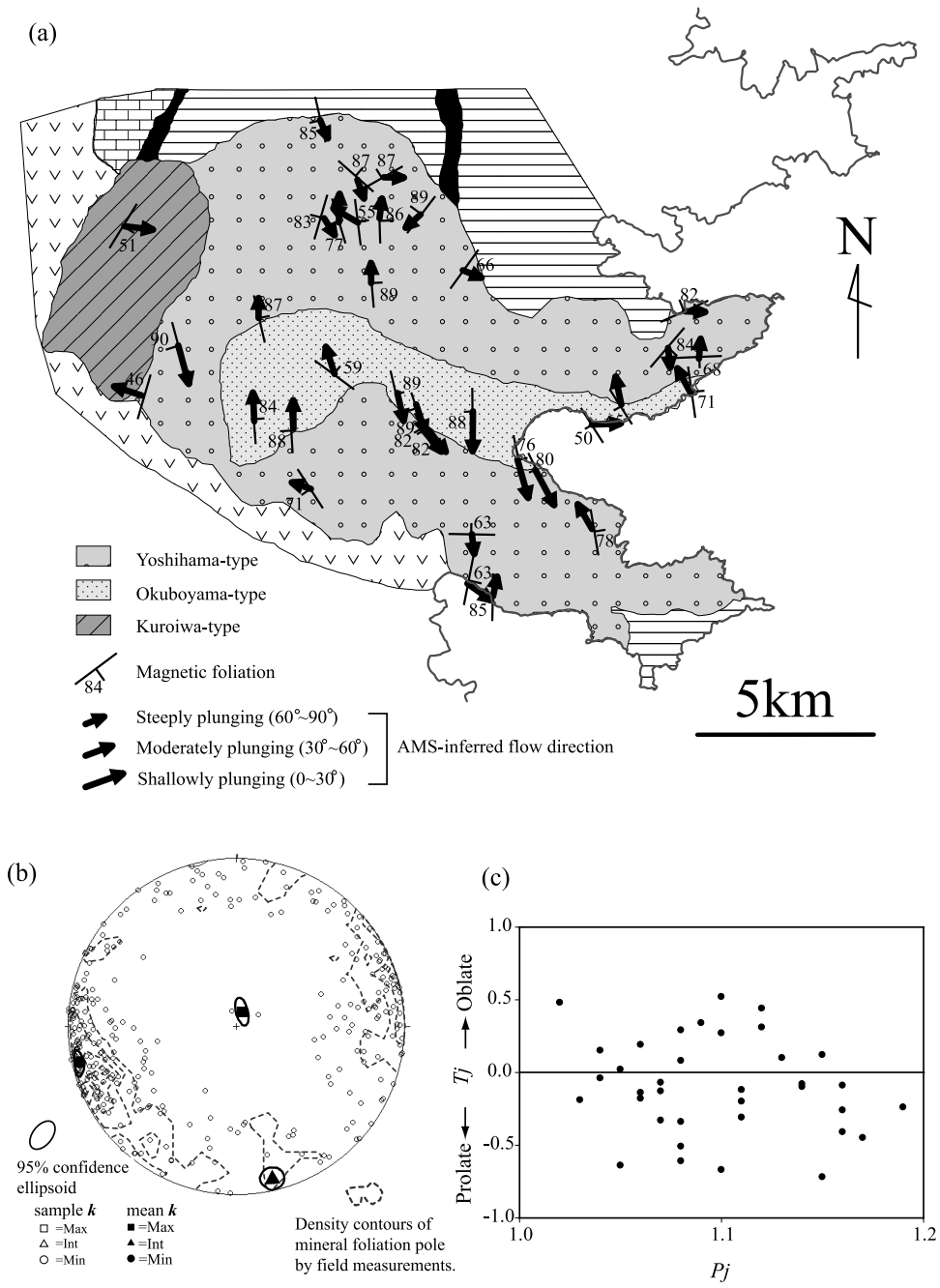

Figure 6. AMS fabrics of the Goyozan plutonic complex and inferred emplacement flow directions for the Goyozan pluton. (a) Map of AMS foliation and lineation. Magnetic lineations are described by three different lengths as shallowly plunging, moderately plunging and steeply plunging, showing an inferred flow direction. (b) Lower hemisphere stereoplot of a sample's principal axes (open squares, maximum; open triangles, intermediate; and open circles, minimum) of AMS with 95% confidence limit ellipsoids (solid line) [*Jelinek*, 1978] superimposed on the density contours of poles to a mineral foliation plane defined in the field (dashed lines). Mean AMS principal axes are shown by a solid square for maximum, solid triangle for intermediate, and solid circle for minimum. Note the coaxiality between AMS mean minimum principal axis and high-density contour of mineral foliations. (c) Plots of the shape parameter T_j versus the degree of anisotropy P_j [*Jelinek*, 1978] of AMS.

addition, we examine one sample from all stations and compare a background-subtracted ApARM tensor with the unsubtracted tensor. For 15 combinations (GG04-medium, GG04-fine, GG09-fine, GG37-medium, GG59-coarse, GG59-fine, GG66-coarse, GG66-medium, GG66-fine, GG73-coarse, GG73-medium, GG73-fine, GG87-medium, GG87-fine and GG104-coarse), their principal orientations of background-subtracted ApARM tensors deviated more than 20°From that of unsubtracted ApARM tensors due to the presence of high-coercive minerals such as hematite.

Table 2a. ApARM Data

Site	Rock Type	Number of Core	Dec/Inc			ARM M, mA/m, 10^{-6} SI	P_j	T_j	Type
			Site Mean Max	Site Mean Int	Site Mean Min				
				Coarse-Grained ApARM Data					
15	Yoshihama	4	134.1/49.3	29.8/39.6	34.6/8.1	30.9	1.77	0.02	I
27	Yoshihama	4	129.3/53.3	9.6/20.3	267.7/29.1	48.3	1.45	0.29	I
35	Yoshihama	5	74.8/74.9	343.1/0.4	253.0/14.1	64.2	1.68	−0.18	I
45	Yoshihama	3	182.0/70.2	327.7/16.55	60.9/10.6	20.5	1.83	−0.36	I
56	Yoshihama	4	43.6/20.0	227.3/69.9	134.0/1.2	27.2	1.48	0.12	I
59	Yoshihama	6	116.7/86.8	239.5/1.8	329.6/2.7	28.0	1.52	−0.02	I
9	Okuboyama	6	344.7/74.0	142.2/14.8	233.7/5.9	272.4	1.50	−0.20	I
17	Okuboyama	7	41.2/41.2	195.9/23.4	290.2/9.7	144.0	1.52	0.07	I
37	Okuboyama	6	358.8/43.2	157.0/44.7	258.2/11.1	123.3	1.52	−0.10	I
70	Okuboyama	5	187.8/17.5	342.1/70.8	95.3/7.8	218.6	1.69	0.15	I
				Medium-Grained ApARM Data					
4	Yoshihama	4	186.6/45.5	329.8/38.2	75.8/19.3	10.9	1.30	0.22	I
15	Yoshihama	4	135.6/38.9	352.2/44.9	241.9/19.2	44.9	1.36	0.01	I
27	Yoshihama	4	102.5/55.6	333.2/23.5	232.2/23.7	168.6	1.22	−0.48	I
35	Yoshihama	5	92.9/72.7	333.9/8.6	241.6/14.9	104.1	1.27	0.04	I
45	Yoshihama	3	208.9/66.2	90.9/11.7	−3.5/20.4	75.3	1.49	0.04	I
56	Yoshihama	4	44.2/48.1	230.5/41.8	137.7/3.2	38.0	1.21	0.01	I
87	Yoshihama	4	249.1/39.9	340.6/1.8	72.7/50.0	19.2	1.48	−0.02	I
104	Yoshihama	4	184.8/57.7	29.9/29.8	293.311.4	277.3	1.28	−0.08	I
9	Okuboyama	6	−4.0/84.9	156.5/4.9	246.6/1.7	409.5	1.32	−0.34	I
17	Okuboyama	7	142.6/46.1	321.2/43.9	51.9/0.7	180.0	1.23	0.02	I
70	Okuboyama	5	183.6/6.3	−2.3/83.7	93.5/07	394.3	1.37	−0.27	I
73	Kuroiwa	4	104.7/41.7	347.6/27.1	235.6/36.3	120.1	1.31	−0.03	I
				Fine-*Grained ApARM Data*					
15	Yoshihama	4	40.9/23.3	289.7/39.9	152.9/41.0	36.9	1.25	−0.47	I
27	Yoshihama	4	91.8/1.5	204.7/86.3	0.7/3.4	775.5	1.60	0.45	II
35	Yoshihama	5	59.9/26.4	184.8/49.0	314.0/28.8	180.6	1.17	0.18	II
45	Yoshihama	3	80.4/13.5	217.0/71.8	347.4/12.1	602.2	2.12	0.05	II
56	Yoshihama	4	226.7/42.5	326.3/10.3	67.1/45.1	39.7	1.18	−0.20	I
104	Yoshihama	4	246.0/34.7	342.7/9.6	85.9/53.6	148.1	1.20	−0.31	II
17	Okuboyama	7	142.6/46.1	321.2/43.9	51.9/0.7	68.0	1.26	0.07	I
37	Okuboyama	6	26.3/18.4	168.9/67.3	291.9/12.9	86.8	1.18	0.00	I
70	Okuboyama	5	182.4/0.1	272.5/58.6	92.4/31.5	139.3	1.18	0.03	I

Thus we discard them from the present analysis. The remaining 30 combinations have only negligible background remanence, accepting ARM vectors in the directions imposed in each step of the experiment.

4.2.2. ApARM Results

[16] Table 2a summarizes ApARM fabric data for three different coercivity windows. Selected data of five stations are shown on corresponding AMS projection in Figure 7. At all stations, ApARM orientations of coarse-grained magnetite and medium-grained magnetite are coaxial (Table 2a). Comparison of AMS fabric with coarse-ApARM and medium-ApARM fabrics indicates similar fabric symmetries. The coaxiality indicates strong control of coarse-grained and medium-grained magnetite on AMS. This result agrees well with the mesoscopic mineral alignment under the optical microscope (Figure 4). We define these coaxial-type data as type I in Table 2a, where AMS appear to be a reliable petrographic marker.

[17] Fine-ApARM fabrics were well defined at five of nine stations (GG27, GG35, GG45, GG70 and GG104), where each of the three principal axes from specimens form a cluster, or one axis forms a cluster and the other two form a girdle. Table 2b shows the maximum and minimum radii of the elliptical 95% confidence cone for these five stations. For another four stations (GG15, GG17, GG37 and GG56), the fabric were scattered within stations and average partial ARM intensity was low, suggesting the absence of fine-grained magnetite inclusions. The stations GG37 and GG70 show that the fine-ApARM fabric is coaxial with AMS, coarse- and medium-ApARM, although GG70 might show

Figure 7. Lower hemisphere stereoplots of AMS, coarse-, medium-, and fine-ApARM fabric with 95% confidence ellipsoids of mean tensor [*Jelinek*, 1978], together with three different types of coercivity spectra (type I for GG17 and type II for GG27 and GG35). The spectrum of type I shows lower intensity in high-coercivity part than type II, implying lower content of fine-grained magnetite. At all stations, AMS foliation and ApARM foliations of coarse-grained magnetite and medium-grained magnetite are coaxial, suggesting a strong control of coarse-grained and medium-grained magnetite on AMS. Type I is defined by the coaxiality among AMS and coarse, medium, and fine ApARM or by random fine-ApARM fabric, suggesting the absence of fine-grained magnetite. Type II is defined by the noncoaxiality between AMS and fine ApARM. Open squares, triangles, and circles are specimen's maximum, intermediate, and minimum tensor axes, respectively. Solid square, triangle, and circle are sample-mean maximum, intermediate, and minimum tensor. Dashed line is magnetic foliation.

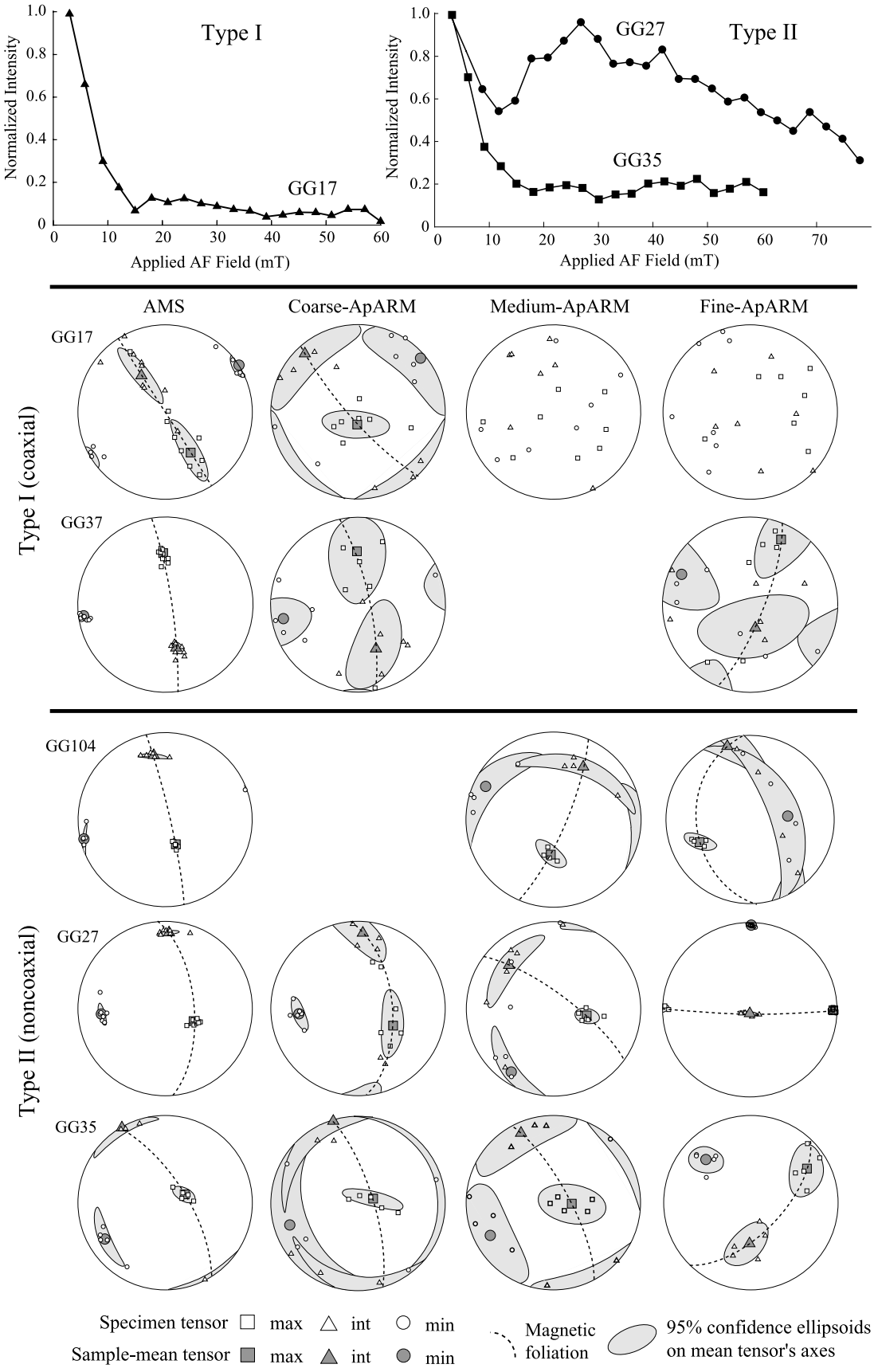
Type I
Normalized Intensity
GG17
Applied AF Field (mT)
Type II
GG27
GG35
AMS
Coarse-ApARM
Medium-ApARM
Fine-ApARM
Type I (coaxial)
GG37
GG104
Type II (noncoaxial)
Specimen tensor max int min
Sample-mean tensor max int min
Magnetic foliation
95% confidence ellipsoids on mean tensor's axes

Figure 7

Table 2b. Radii of 95% Confidence Ellipses of Type II Fine-ApARM Fabric

	Max		Int		Min	
Site	α_{95}(max)	α_{95}(min)	α_{95}(max)	α_{95}(min)	α_{95}(max)	α_{95}(min)
27	8	4	8	2	4	2
35	26	16	25	12	18	12
45	7	2	8	2	9	5
104	18	7	87	15	86	16
70	28	17	74	8	76	27

noncoaxiality with AMS if the mean minimum axis is interchangeable with intermediate one. We also define these scattered-type and coaxial-type data as type I in Table 2a. For GG27, GG35, GG45 and GG104, fine-ApARM fabrics were oblique to the AMS fabric that is parallel to the preferred alignment of mafic minerals. Both magnetic lineation and foliation were different between coarse- and medium-ApARMs and fine-ApARM fabrics (Figure 7). These noncoaxial-type data are defined as type II in Table 2a. AMS, coarse- and medium-ApARM fabrics usually have steep to moderate dips of lineation and NNW-SSE strikes of foliation, while fine-ApARM fabric shows a low dip of lineation and E-W to NE-SW strike of foliation. Fabric symmetries for ApARM are shown in Figure 8. Because the fabric symmetry of medium ApARM of GG27 is prolate, the interchange between the intermediate and minimum axes causes the foliation to be coaxial with the AMS fabric. Generally, if the fine-ApARM fabric is nearly oblate (prolate), the maximum (intermediate) axes are interchangeable with intermediate (minimum) axes so that maximum axes scatter along the foliation plane. However, the oblate fabrics of fine ApARM (GG27, GG35 and GG45) deflect noncoaxially from the foliation plane for AMS and coarser ApARM fabrics, even after interchanging the maximum axes to the intermediate ones. This deflection implies a difference in alignment between mafic minerals and fine-grained magnetite, and highlights the need for an independent check of the difference. We performed scanning electron microscope (SEM) observation to characterize the source of the oblique fine-ApARM fabric.

5. Iron Oxide Mineralogy: SEM Observation

[18] Under the optical microscope, coarse-grained and medium-grained magnetites were found to be euhedral primary grains (Figures 4d and 4e). On the other hand, fine-grained magnetite of coercivity of 15–60 mT is considered to be too small to observe under the optical microscope [*Dunlop and Özdemir*, 1997]. Thus the occurrence of fine-grained magnetite was investigated through SEM. SEM observation shows that needle-shaped magnetite is mostly found as oxide microexsolution rods in clinopyroxene and plagioclase (Figures 9a and 9b). The magnetites generally have strong shape anisotropy with width less than 2 μm and length between 2 and 10 μm (Figures 9a and 9b). The energy dissipative spectroscopy analyses show iron as the only cation; they are titanium free. Even though they are larger than 0.1 μm, their extreme shape anisotropy supports a single-domain behavior [*Butler and Banerjee*, 1975]. The fine-grained magnetite is also found along randomly orientated microfractures (Figure 9c) but far less common than exsolution grains. Thus it is likely that a fine-ApARM fabric is influenced more by magnetite microexsolutions in clinopyroxene and plagioclase than by fine-grained inclusions in microfractures. In addition, clinopyroxene crystals were only found in samples from the station where the fine ApARM were well defined. The microexsolutions of fine-grained magnetite have a strong preferred orientation within host crystals. Most needle-shaped fine-grained magnetites are elongated parallel to the {010} twin plane of plagioclase crystals, in most cases they are the longest dimension of the host crystals (Figures 4 and 9). Because ApARM is free from the "AMS-inverse effect" of fine single-domain grains, the preferred orientation of fine-grained magnetite is dictated by the crystal symmetry of the host crystals of plagioclase and clinopyroxene. Since the host crystals possess a preferred orientation that was produced by magmatic and submagmatic flow, the fine-ApARM fabric correlates with the preferred orientation of plagioclase and clinopyroxene crystals. In order to confirm this correlation, we have compared magnetic anisotropies with plagioclase and mafic mineral petrofabrics determined by image analysis.

6. Comparison of Fine-ApARM Fabric With Petrofabrics and AMS

[19] Figure 7 and Table 2a show that fine-ApARM fabric (type II) is oblique to AMS in GG27, GG35, GG45 and GG104. In order to explore the petrofabric of this obliquity, we prepared two large thin sections of 4 cm × 2 cm from a typical sample GG27 cut parallel to the AMS k_1–k_3 plane

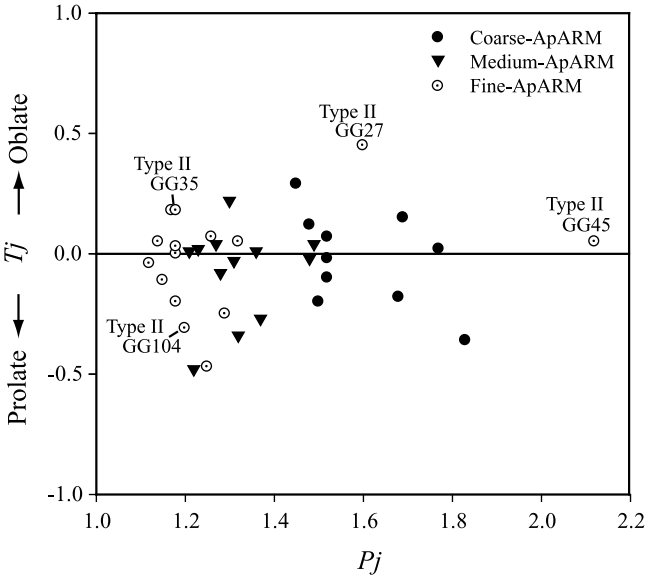

Figure 8. Plot of the shape parameter T_j versus the degree of anisotropy P_j for coarse ApARM (solid circle), medium ApARM (solid reverse triangle), and fine ApARM (open double circle). ApARM fabrics show triaxial to prolate symmetries and stronger degree of anisotropy than AMS, indicating that ApARM fabrics are contributed by needle-shaped magnetite.

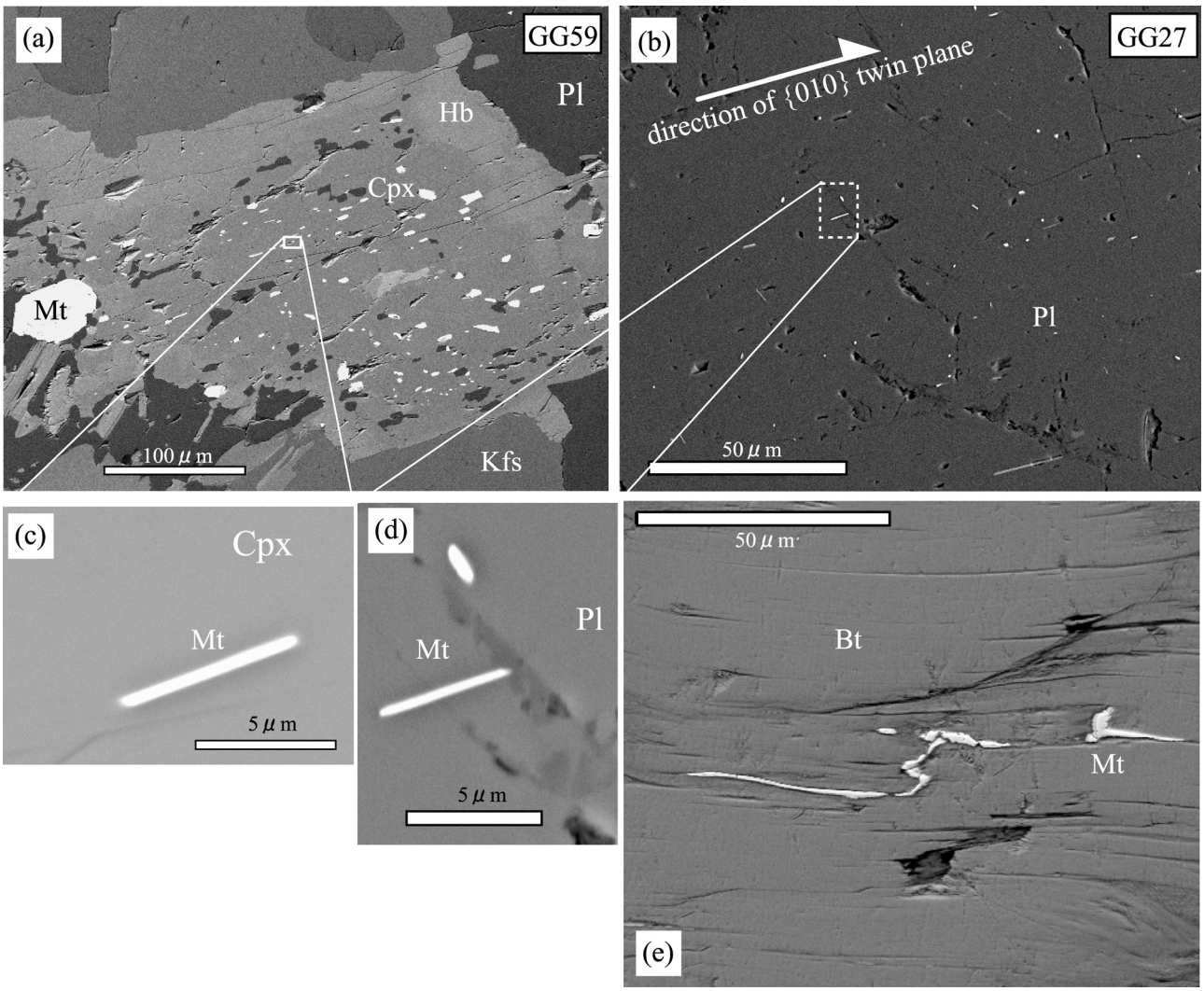

Figure 9. Backscattered electron (BSE) images of fine-grained magnetite inclusions hosted in clinopyroxene and plagioclase. (a) Micron-sized needle-shaped magnetite inclusions hosted in clinopyroxene with euhedral medium-grained magnetite. (b) Micron-sized needle-shaped magnetite inclusions hosted in plagioclase. (c, d) Magnified image of a magnetite grain in Figures 9a and 9b. These needle-shaped magnetites show strong shape anisotropy with width less than 2 μm and length between 2 and 10 μm, indicating a single-domain-like behavior. (e) Oxide-filled microfracture in biotite. Microfractures with oxide are less common compared to the needle-shaped magnetites. Cpx, clinopyroxene; Pl, plagioclase; Mt, magnetite; Bt, biotite.

and k_2–k_3 plane. In GG27, k_1 and k_3 is almost identical to the principal axes of fine-ApARM of intermediate ($A_{\text{int-Fine}}$) and maximum ($A_{\text{max-Fine}}$) direction, respectively (see Figure 10a). The thin sections can be regarded as the $A_{\text{int-Fine}} - A_{\text{max-Fine}}$ plane and the $A_{\text{min-Fine}}$ (minimum axis of fine-ApARM) $- A_{\text{max-Fine}}$ plane, respectively (Figures 10b and 10c). If the fine-ApARM fabric reflects the preferred orientation of magnetite inclusions in plagioclase, the preferred elongation of plagioclase should lie along $A_{\text{max-Fine}}$ axis in both thin sections and should not along $A_{\text{int-Fine}}$ axis. We traced the elongation orientation of twin lamella in whole plagioclase crystals on thin sections under an optical microscope. Moreover, to check mafic minerals fabrics, we also traced the elongation orientations of hornblende and biotite under optical microscope (Figures 10b and 10c). Then all of the orientations were counted and evaluated on rose diagrams (Figures 10b and 10c). These indicate that the preferred elongation of plagioclase on both thin section planes matches the $A_{\text{max-Fine}}$ direction, not the k_1 axis of AMS. This supports the view that fine ApARM reflects the flow aligned, preferred orientation of plagioclase. In addition, it is implied that AMS does not correspond with petrofabric flow alignments of plagioclase crystals in the Goyozan granitoid. On the other hand, the hornblende and biotite alignments are mostly perpendicular to the plagioclase alignment (Figures 10b, 10c, and 10d). Figure 11 shows that biotite and coarse-grained magnetite crystallized in interstitial spaces of plagioclase with quartz, being perpendicular to the plagioclase twin orientations. This supports an observed good directional correlation among

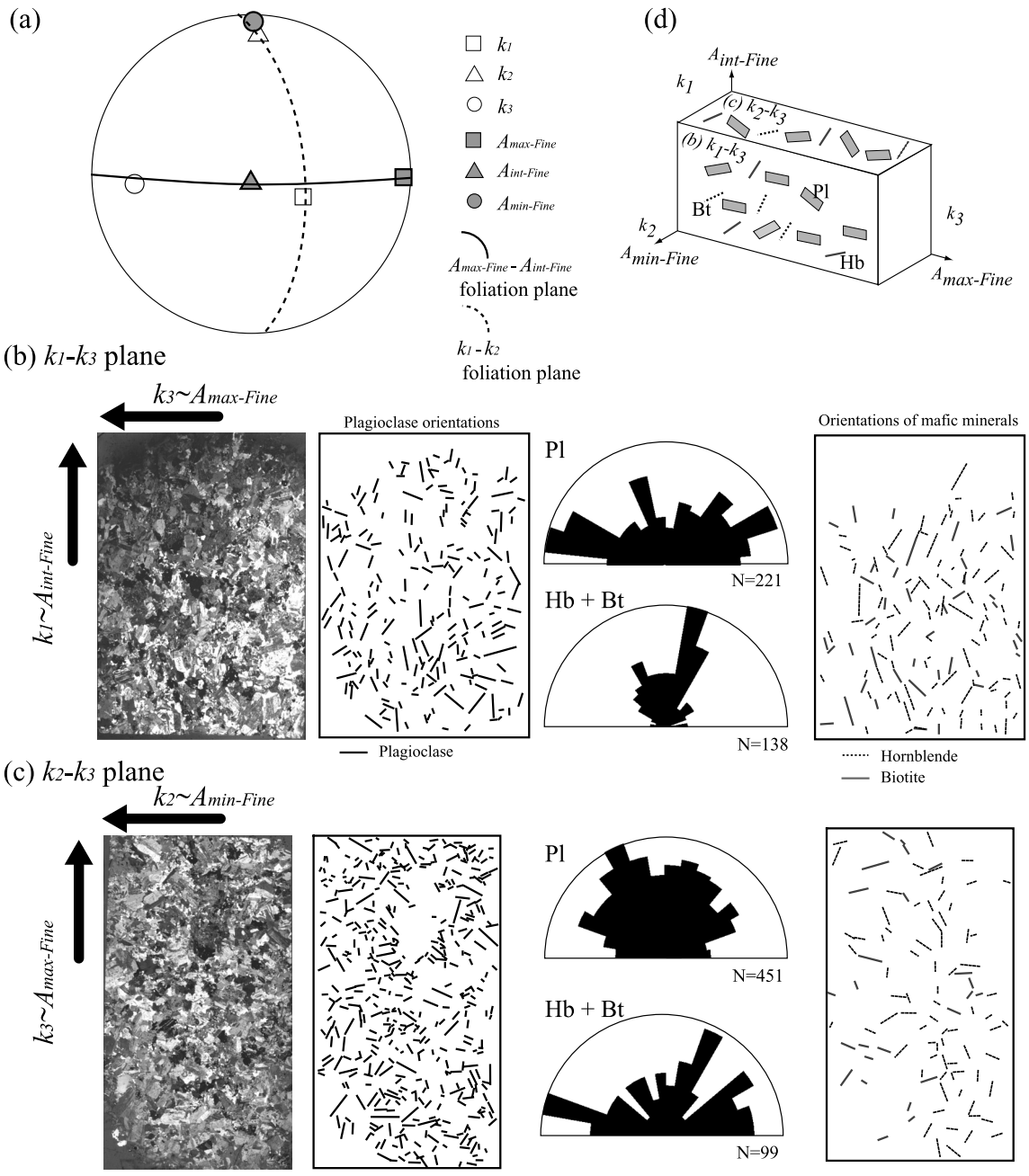

Figure 10. Image analysis of preferred orientation of plagioclase and mafic silicate (hornblende and biotite) crystals on large oriented thin sections of a specimen from GG27. (a) Orientation relationship of thin sections. The k_1, k_2, and k_3 are nearly correspondent to maximum ($A_{\text{int-Fine}}$), intermediate ($A_{\text{min-Fine}}$), and minimum ($A_{\text{max-Fine}}$) principal axes of fine-ApARM fabric, respectively. (b) A photomicrograph of the thin section cut parallel to the k_1–k_3 plane of AMS ellipsoid, an extracted orientation of plagioclase twins, rose diagram of plagioclase and mafic minerals, and an extracted orientation of hornblende and biotite. The preferred plagioclase elongation matches the $A_{\text{max-Fine}}$ direction, not the k_1 axis of AMS. Mafic silicates of hornblende and biotite show preferred orientation along k_1. This implies that the plagioclase fabric is perpendicular to the mafic minerals fabric. (c) A photomicrograph of the thin section cut parallel to the k_2–k_3 plane of AMS ellipsoid, an extracted orientation, rose diagram of plagioclase and mafic minerals, and an extracted orientation of hornblende and biotite. The preferred plagioclase elongation matches the $A_{\text{max-Fine}}$ direction. Mafic silicates show preferred orientation along k_2. (d) Schematic representation of the determined preferred orientations of minerals with respect to magnetic principal axes. Plagioclase crystals have a preferred orientation along k_3 ($A_{\text{max-Fine}}$), while mafic silicate are aligned along k_1 ($A_{\text{int-Fine}}$).

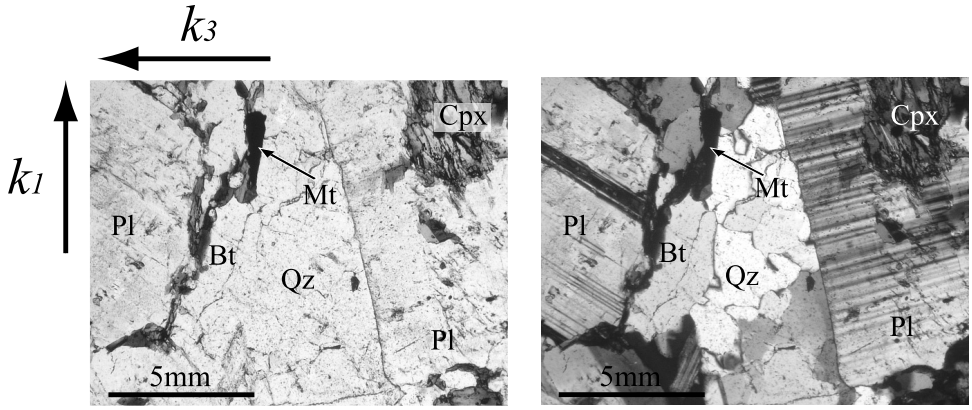

Figure 11. Photomicrographs (transmitted light) of a thin section from GG27 showing a textural relationship among plagioclase, clinopyroxene, quartz, biotite, and magnetite. Quartz, biotite, and magnetite appear as anhedral crystals in interstitial space between plagioclase and clinopyroxene. Note that the orientation of biotite and magnetite grains is nearly parallel to the AMS k_1 axis, being perpendicular to plagioclase twin orientations.

mafic minerals, magnetite and AMS fabrics. Marked deviations between the AMS and fine-ApARM fabric directions can be accounted for by careful examination of the sample.

7. Discussion

[20] Previous ApARM studies showed that the ApARM fabric of fine-grained magnetite is believed to be of secondary origin from the observation of sets of microfractures decorated by iron oxides [*Trindade et al.*, 1999, 2001; *Diot et al.*, 2003; *Bolle et al.*, 2003]. They revealed changes in fabrics that are ascribed to the secondary geological process from the comparison between unaltered granitoid and hydrothermally altered granitoid, which is similar to a direct correlation between AMS and the fractal dimension of fault zone microfractures in granitoid [*Nakamura and Nagahama*, 2001]. Moreover, *Giroux and Benn* [2005] also interpret fine-grained magnetite in dioritic dikes in Sudbury Structure to be of secondary origin, formed during static greenschist-grade metamorphic replacement of biotite by chlorite. However, not all the fine-grained magnetites are of secondary origin. In many igneous rocks, the microscopic ferromagnetic grains that carry the best paleomagnetic signal are exsolved as microinclusions within a host mineral [*Evans and McElhinny*, 1966; *Hargraves and Young*, 1969; *Murthy et al.*, 1970; *McClay*, 1974; *Davis*, 1981; *Renne and Onstott*, 1988; *Xu et al.*, 1997; *Feinberg et al.*, 2005]. This suggests that the oblique fabrics between plagioclase and AMS fabric are explained in terms of their mineral carriers and fabric development processes. Because the magnetite inclusions are generally either parallel or perpendicular to the {010} twin grown under minimum interface energy [*Fleet*, 1982], the orientation of the exsolved inclusions should follow the elongated direction of host crystals of plagioclase or clinopyroxene, although *Fleet* [1982] revealed that the inclusions likely developed after crystallization of primary silicates at about 600°C. Moreover, the silicate host protects the magnetite inclusions from chemical alteration by hydrothermal fluids. Therefore, although the posttectonic or syntectonic overprinting to AMS fabric appears to mask the fabric of low-susceptibility plagioclase in the Goyozan granitoid, the fine-ApARM fabric of our samples apparently isolates the preferred orientation of framework-forming silicates of plagioclase or clinopyroxene, without image analysis [*Cruden et al.*, 1999].

[21] The origin of the discrepancy between AMS and plagioclase in the Goyozan granitoid may be similar to that suggested by *Launeau and Cruden* [1998]. Because crystallizing magmas are considered as dynamic fluid systems in which particles nucleate and grow, we examine a magma emplacement process of the Goyozan granitoid from modeled phase relationships in silicate-water systems (Figure 12a) and viscosity of crystallizing granular flow systems (Figure 12b). A magma differentiation scheme during the emplacement of Goyozan-type granitoids is considered as follows:

[22] 1. framework-forming silicates (plagioclase, hornblende and clinopyroxene) crystallize from a magmatic melt (Figures 12a and 12b). Enough melt is present for the crystal to be independent of its neighbors and rotate toward the flow direction (i.e., magmatic flow).

[23] 2. As crystallization proceeds, opportunities for further rotation and growth of early phases diminish because of the interaction with neighboring grains (i.e., submagmatic flow). Late crystallizing minerals such as magnetite, quartz and biotite would be forced to grow into spaces whose shape depends on the early crystallized framework of silicate minerals [*Bryon et al.*, 1994]. These late crystallizing minerals may rotate during local flow, due to their small size. In addition, external force may produce microstructures such as microfractures or microveins during this regime [*Hibbard*, 1980; *Bouchez et al.*, 1992].

[24] 3. After full crystallization, needle-shaped magnetite inclusions exsolved along plagioclase twin lamella. During these continuum emplacement processes, Goyozan granitoids were formed by intrusion of silicic plutons into Paleozoic and Mesozoic basement rocks in response to the westward subduction of the oceanic Pacific plate. Therefore the timing of fabric acquisition should be considered with respect to the crystallization history of the magma during emplacement. Thus the framework-forming silicates most likely acquired their preferred orientation in a

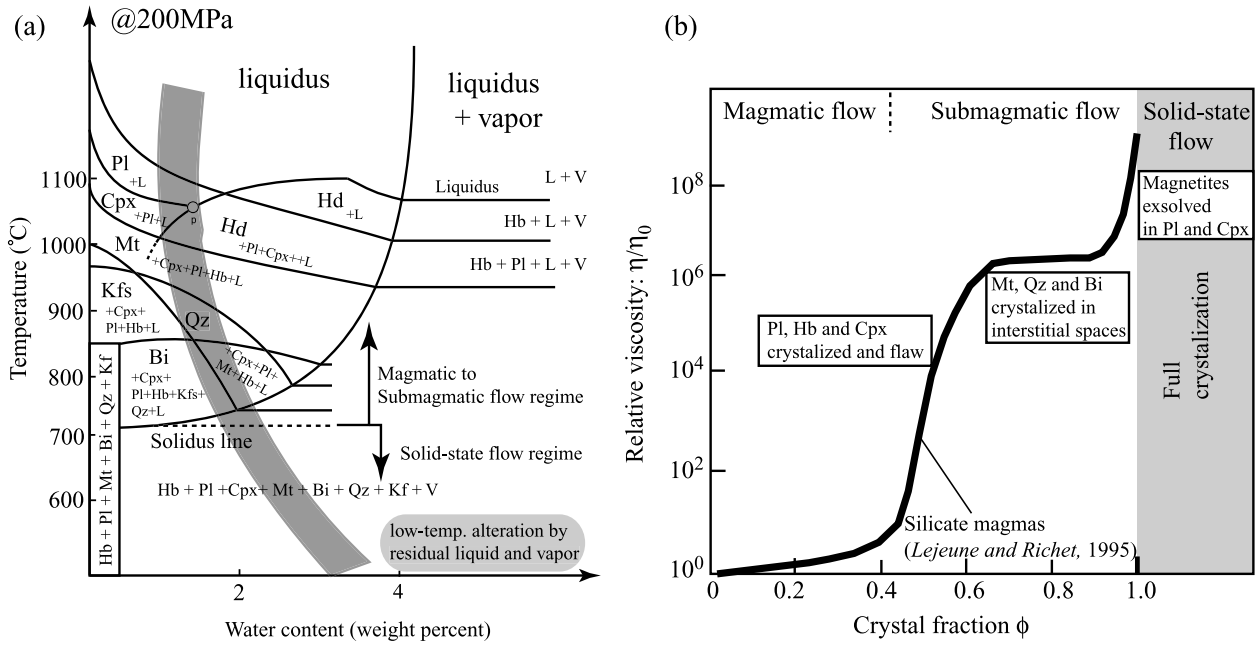

Figure 12. (a) Schematic isobaric temperature-water contents projection at 200 MPa for modeled Goyozan granodiorite showing the estimated upper stability limits for individual minerals (redrawn from *Robertson and Wyllie* [1971]). Shaded line shows an equilibrium path of magma differentiation in Goyozan granitoids. L, liquid; V, vapor; Pl, plagioclase; Cpx, clinopyroxene; Hd, hornblende; Mt, magnetite; Qz, quartz; Bi, biotite; and Kfs, alkali feldspar. Dotted solidus line may be a flow regime boundary between magmatic flow and solid-state flow. (b) Schematic granular flow diagram during a magma differentiation of Goyozan granitoid in relation to relative viscosity (η/η_0) and crystal fraction (ϕ) in a melt (redrawn from *Lejeune and Richet* [1995] and *Blenkinsop* [2000]). The melt fractions and viscosity changes in the transitions from magmatic through submagmatic to solid-state flow are schematic and vary with magma composition. Viscosity relations are shown from the experiments of *Lejeune and Richet* [1995] on silicate magmas. Examination of the equilibrium path of Goyozan granitoids suggests the following magma differentiation scheme: (1) Framework-forming silicates (plagioclase, hornblende and clinopyroxene) have been crystallized from a magmatic melt in a magmatic to submagmatic flow regime of the Goyozan granitoids. (2) As crystallization proceeds, late crystallizing minerals such as magnetite, quartz, and biotite were forced to grow into interstitial spaces. (3) After full crystallization, needle-shaped magnetite inclusions exsolved along plagioclase twin lamella.

magmatic and submagmatic flow in which the silicate laths were interacting strongly, forming WNW-ESE to E-W foliations with moderate to shallow dip by the rotation of the silicates through a lateral spreading of magma to the east. This framework-forming silicate fabric can be traced by magnetite microexsolutions along the twin plane in plagioclase and clinopyroxene, using fine ApARM. On the other hand, AMS may reflect a flow-induced local inversion of late crystallized coarse- and medium-grained magnetite and biotite. The N-S to NNW-SSE foliation of AMS in the Yoshihama-type granitoid may have resulted from local flow of residual melt and development of microstructures under an E-W transpressional tectonic setting during the early Aptian [*Kanagawa*, 1986]. An important implication of this interpretation is that the ApARM has the potential to show not only the later alteration history but also the emplacement and crystallization dynamics of granitic rocks. That may be impossible from AMS alone.

[25] Previous field studies of mafic mineral alignments in this Goyozan granitoid and gravity surveys suggested that a magmatic feeder zone lay in the northern part of the granitoid. Subsequently, the granitic magma flowed to the eastern boundary. In the southern wall boundary of the granitoid, however, the AMS, coarse- and medium-ApARM lineations also plunge steeply, suggesting another cryptic magmatic feeder zone. In contrast to AMS, coarse- and medium-ApARM fabrics, fine-ApARM fabric indicates a subhorizontal flow fabric, matching the preferred orientation of plagioclase laths (Figure 13). Therefore fine-ApARM fabrics more reliably proxy for the flow pattern since they correlate directly with the flow-aligned plagioclase subfabric. On the other hand, AMS on its own masks the true magnetic flow fabric due to competing subfabrics and the field measurement of ill-defined foliations is still less reliable [*Diot et al.*, 2003; *Bolle et al.*, 2003]. Moreover, the fine-ApARM fabric provides an alternative interpretation for the source of the noncoaxial plagioclase and AMS, due to flow-induced local inversion of magnetite and mafic minerals [*Cruden et al.*, 1999]. Also it unveils the flow nature of low-susceptibility silicates that have been masked by the posttectonic or syntectonic overprinting to AMS fabric [*Pignotta and Benn*, 1999].

[26] The present study investigates grain-size-related anisotropies of magnetite by ApARM, foliation of mafic

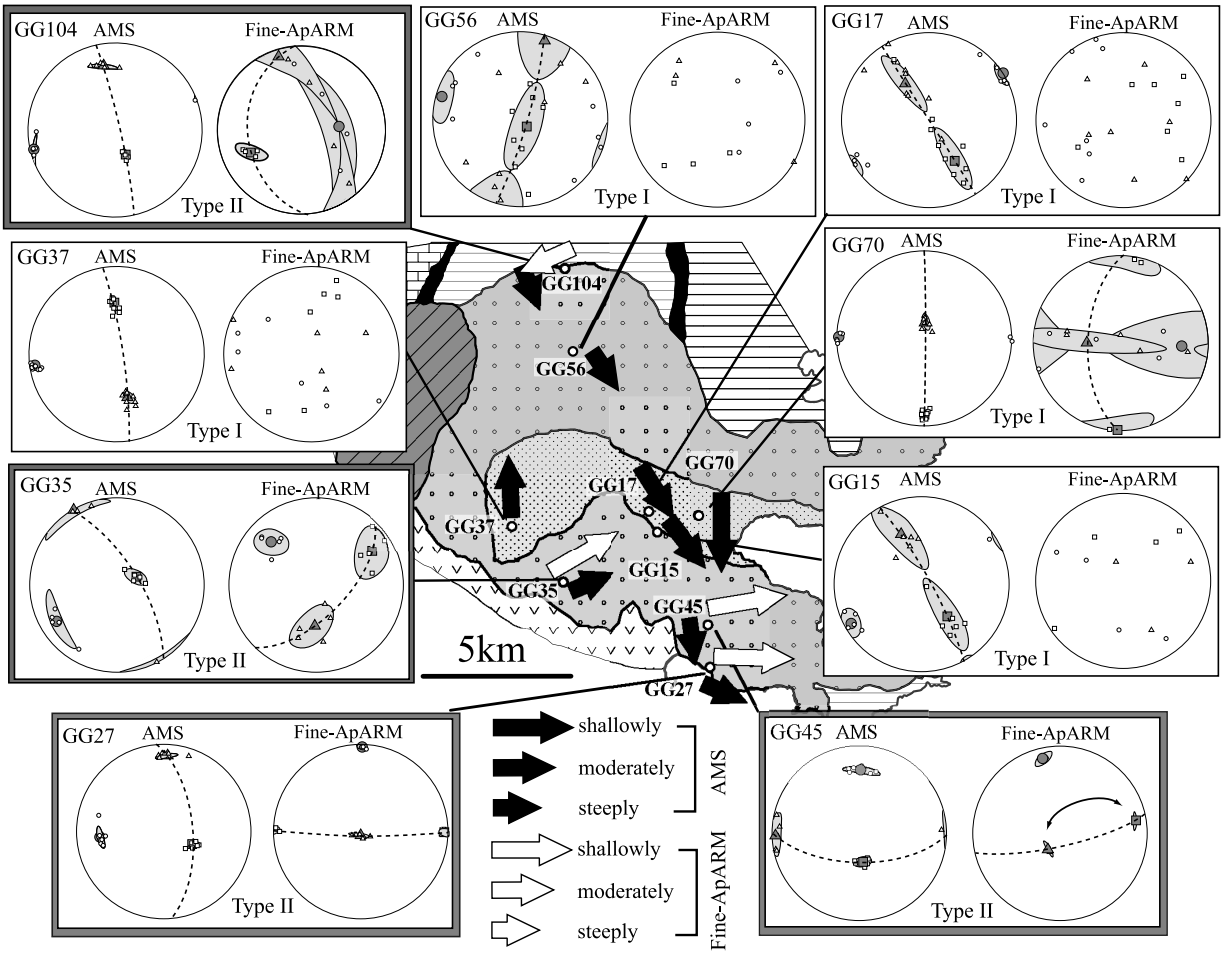

Figure 13. Map of magnetic anisotropies fabric and inferred emplacement flow directions for the Goyozan plutonic complex. Equal-area lower hemisphere fabric projections of AMS and fine ApARM are provided for all ApARM sampling stations. Solid arrows provide AMS-inferred magmatic flow directions (magnetic lineations) of three different lengths as shallowly plunging, moderately plunging and steeply plunging. Type I stations show a coaxiality between AMS and medium- and coarse-ApARM fabrics, where AMS appear to be a reliable petrographic marker. These AMS-inferred flow directions are parallel to the alignments of hornblende, biotite, and coarse magnetite. Type II stations (double-lined box) demonstrate a noncoaxial fabric between AMS and fine ApARM. For type II stations, fine-ApARM lineations (open arrows) suggest shallowly plunging magmatic flow directions, which contradict with the AMS-inferred flow. Fine-ApARM fabric indicates the orientation of plagioclase crystals (Figure 10), and their shallow plunging and nearly E-W directions are in better agreement with the emplacement model of the complex (Figure 3), where magma spread laterally from the north central part of the Yoshihama-type granitoid to the SE and east direction.

silicates by field survey, and preferred orientation of plagioclase and mafic minerals by optical microscope. Field-determined foliation, coarse ApARM, medium ApARM, and AMS are coaxial (Figures 1, 4, and 5). The coaxiality between coarse ApARM and medium ApARM dismiss the effect of stress-induced alignment of the domain wall [*Borradaile and Kehlenbeck*, 1996] on magnetic anisotropy of coarse-grained magnetite in the plutons. On the other hand, some fine-ApARM fabrics are oblique to AMS fabric. SEM investigation and optical petrofabric observation revealed that fine ApARM is carried by needle-shaped magnetite microexsolutions in plagioclase and clinopyroxene, and reflect the preferred orientation of elongated laths of plagioclase and clinopyroxene. In the Goyozan granitoid, early crystallized low-susceptibility silicates were camouflaged by preferred dimensional orientation of high-susceptibility magnetite as well as by the preferred shape orientation of mafic silicates. Moreover, Figure 10 showed that the AMS maximum axis does not match the preferred orientation of the long axis of plagioclase, which includes fine-grained magnetites along their {010} twin planes. Therefore, in rocks with multiple mineralogical sources of susceptibility, AMS need not bear a simple relationship to the primary flow fabric of low-susceptibility plagioclase. This shows that AMS must be interpreted carefully in

structural analysis of granitoid, even though AMS and the petrofabric of mafic silicates may be similar.

8. Conclusions

[27] The combined use of ApARM fabric isolation for magnetite and SEM observation leads us to interpret that fine-grained magnetite fabric is only partly due to secondary geological process such as hydrothermal alteration. For the most part, it is a proxy for the alignment of silicate crystals that bear magnetite microexsolutions. This alignment occurred during magmatic and submagmatic flow regimes, giving an apparent magmatic flow direction of a granitoid. Our petrofabric analysis of oriented thin sections revealed that the preferred orientation of plagioclase's long axes differs from the orientation of AMS principal axes that are parallel to the field observation of mafic mineral alignments. These results suggest that the presence of exsolved magnetite inclusions hosted in plagioclase and clinopyroxene allows fine-ApARM fabric to be a reliable marker for determining the orientation of magmatic flow direction of Goyozan granitoids.

[28] **Acknowledgments.** We are grateful to G. J. Borradaile for improving the early version of the manuscript and for correcting English grammar. Gorjan Paul refined our English grammar. Constructive reviews by R. J. Enkin, K. Benn, and C. Archanjo helped to improve the manuscript. This work was partially supported by the 21st century Center-Of-Excellence (COE) program (Earth Sciences) at Tohoku University and the Ministry of Education, Science, Sports and Culture grant-in-Aid for Young Scientists (B).

References

Archanjo, C. J., and P. Launeau (2004), Magma flow inferred from preferred orientations of plagioclase of the Rio Ceará-Mirim dyke swarm (NE Brazil) and its AMS significance, in *Magnetic Fabric: Methods and Applications*, edited by F. Martín-Hernández et al., *Geol Soc. Spec. Publ.*, *238*, 285–298.

Archanjo, C. J., P. Launeau, and J. L. Bouchez (1995), Magnetic fabric vs. magnetite and biotite shape fabrics of the magnetite-bearing granite pluton of Gameleiras (northeast Brazil), *Phys. Earth Planet. Inter.*, *89*, 63–75.

Archanjo, C. J., M. G. S. Araujo, and P. Launeau (2002), Fabric of the Rio Ceará-Mirim mafic dyke swarm (northeastern Brazil) determined by anisotropy of magnetic susceptibility and image analysis, *J. Geophys. Res.*, *107*(B3), 2046, doi:10.1029/2001JB000268.

Benn, K., P. Rochette, J. L. Bouchez, and K. Hattori (1993), Magnetic susceptibility, magnetic mineralogy and magnetic fabrics in a late Archean granitoid-gneiss belt, *Precambrian Res.*, *63*, 59–81.

Blenkinsop, T. (2000), *Deformation Microstructures and Mechanisms in Minerals and Rocks*, 164 pp., Springer, New York.

Bolle, O., H. Diot, and R. I. F. Trindade (2003), Magnetic fabrics in the Holum granite (Vest-Agder, southernmost Norway): Implication for the late evolution of the Sveconorwegian (Grenvillian) orogen of SW Scandinavia, *Precambrian Res.*, *121*, 221–249, doi:10.1016/S0301-9268(03)00013-5.

Borradaile, G. J. (1994), Paleomagnetism carried by crystal inclusions: The effect of preferred crystallographic orientation, *Earth Planet. Sci. Lett.*, *126*, 171–182.

Borradaile, G. J. (2003), *Statistics of Earth Science Data: Their Distribution in Time, Space and Orientation*, 351 pp., Springer, New York.

Borradaile, G. J., and D. Gauthier (2001), AMS-detection of inverse fabrics without AARM, in ophiolite dikes, *Geophys. Res. Lett.*, *28*, 3517–3520.

Borradaile, G. J., and D. Gauthier (2003), Interpreting anomalous magnetic fabrics in ophiolite dikes, *J. Struct. Geol.*, *25*, 171–182.

Borradaile, G. J., and B. Henry (1997), Tectonic applications of magnetic susceptibility and its anisotropy, *Earth Sci. Rev.*, *42*, 49–93.

Borradaile, G. J., and M. Jackson (2004), Anisotropy of magnetic susceptibility (AMS): Magnetic petrofabrics of deformed rocks, in *Magnetic Fabric: Methods and Applications*, edited by F. Martín-Hernández et al., *Geol Soc. Spec. Publ.*, *238*, 299–360.

Borradaile, G. J., and M. M. Kehlenbeck (1996), Possible cryptic tectonomagnetic fabrics in 'post-tectonic' granitoid plutons of the Canadian Shield, *Earth Planet. Sci. Lett.*, *137*, 119–127.

Borradaile, G. J., and M. Stupavsky (1995), Anisotropy of magnetic susceptibility: Measurement schemes, *Geophys. Res. Lett.*, *22*, 1957–1960.

Bouchez, J. L., G. Gleizes, T. Djouadi, and P. Rochette (1990), Microstructure and magnetic susceptibility applied to emplacement kinematics of granites: The example of the Foix pluton (French Pyrenees), *Tectonophysics*, *184*, 157–171.

Bouchez, J. L., C. Delas, G. Gleizes, and A. Nédélec (1992), Submagmatic microfractures in granites, *Geology*, *20*, 35–38.

Bouchez, J. L., D. H. W. Hutton, and W. E. Stephens (Eds.) (1997), *Granite: From Segregation of Melt to Emplacement Fabrics*, 358 pp., Springer, New York.

Bryon, D. N., M. P. Atherton, and R. H. Hunter (1994), The description of the primary textures of "Cordilleran" granitic rocks, *Contrib. Mineral. Petrol.*, *117*, 66–75.

Butler, R. F., and S. K. Banerjee (1975), Theoretical single-domain grain-size range in magnetite and titanomagnetite, *J. Geophys. Res.*, *80*, 4049–4058.

Cañón-Tapia, E., G. Walker, and E. Herrero-Bervera (1996), The internal structure of lava flows-insights from AMS measurements I: Near-vent a'a, *J. Volcanol. Geotherm. Res.*, *70*, 21–36.

Cruden, A. R., and P. Launeau (1994), Structure, magnetic fabric and emplacement of the Archean Lebel Stock, SW Abitibi Greenstone Belt, *J. Struct. Geol.*, *16*, 677–691.

Cruden, A. R., O. T. Tobisch, and P. Launeau (1999), Magnetic fabric evidence for conduit-fed emplacement of a tabular intrusion: Dinkey Creek Pluton, central Sierra Nevada batholith, California, *J. Geophys. Res.*, *104*, 10,511–10,530.

Davis, K. E. (1981), Magnetite rods in plagioclase as the primary carrier of stable NRM in ocean floor gabbros, *Earth Planet. Sci. Lett.*, *55*, 190–198.

Day, R., M. D. Fuller, and V. A. Schmidt (1977), Hysteresis properties of titanomagnetites: Grain-size and compositional dependence, *Phys. Earth. Planet. Inter.*, *13*, 260–267.

Diot, H., O. Bolle, J. M. Lambert, P. Launeau, and J. C. Duchesne (2003), The Tellnes ilmenite deposit (Rogaland, south Norway): Magnetic and petrofabric evidence for emplacement of Ti-enriched noritic crystal mush in a fracture zone, *J. Struct. Geol.*, *25*, 481–501.

Dunlop, D., and Ö. Özdemir (1997), *Rock Magnetism: Fundamental and Frontiers*, 573 pp., Cambridge Univ. Press, New York.

Ehiro, M. (1977), The Hizume-Kesennuma fault, with special reference to the character and significance on the geologic development (in Japanese with English abstract), *Contrib. Inst. Geol. Paleontol. Tohoku Univ.*, *77*, 1–37.

Ehiro, M., and S. Kanisawa (1999), Origin and evolution of the South Kitakami Microcontinent during the Early-Middle Paleozoic, in *Gondwana Dispersion and Asian Accretion: IGCP 321 Final Results Volume*, edited by I. Metcalfe, pp. 283–295, A. A. Balkema, Brookfield, Vt.

Ehiro, M., and N. Suzuki (2003), Re-definition of the Hayachine Tectonic Belt of northeast Japan and a proposal of a new tectonic unit (in Japanese with English abstract), the Nedamo Belt, *Astrophys. J. Struct. Geol.*, *47*, 13–21.

Ellwood, B. B., and J. A. Whitney (1980), Magnetic fabric of the Elberton Granite, northeast Georgia, *J. Geophys. Res.*, *85*, 1481–1486.

Engebretson, D. C., A. Cox, and R. G. Gordon (1985), Relative motions between oceanic and continental plates in the Pacific basin, *Spec. Pap. Geol. Soc. Am.*, *206*, 1–59.

Evans, M. E., and M. W. McElhinny (1966), The paleomagnetism of the Modipe Gabbro, *J. Geophys. Res.*, *71*, 6053–6063.

Feinberg, J. M., H. R. Wenk, P. R. Renne, and G. R. Scott (2004), Epitaxial relationships of clinopyroxene-hosted magnetite determined using electron backscatter diffraction (EBSD) technique, *Am. Mineral.*, *89*, 462–466.

Feinberg, J. M., G. R. Scott, P. R. Renne, and H. R. Wenk (2005), Exsolved magnetite inclusions in silicates: Features determining their remanence behavior, *Geology*, *33*, 513–516, doi:10.1130/G21290.1.

Fleet, M. E. (1982), Orientation of phase and domain boundaries in crystalline solids, *Am. Mineral.*, *67*, 926–936.

Fuller, M. (1963), Magnetic anisotropy and paleomagnetism, *J. Geophys. Res.*, *68*, 293–309.

Geoffroy, L., J. P. Callot, C. Aubourg, and M. Moreira (2002), Magnetic and plagioclase linear fabric discrepancy in dykes: A new way to define the flow vector using magnetic foliation, *Terra Nova*, *14*, 183–190.

Girdler, R. W. (1961), The measurement and computation of anisotropy of magnetic susceptibility in rocks, *Geophys. J. R. Astron. Soc.*, *5*, 34–44.

Giroux, L., and K. Benn (2005), Emplacement of the Whistle dike, the Whistle embayment and hosted sulfides, Sudbury Impact Structure, based on anisotropies of magnetic susceptibility and magnetic remanence, *Econ. Geol.*, *100*, 1207–1227.

Grégoire, V., M. De Saint Blanquat, A. Nedelec, and J. L. Bouchez (1995), Shape anisotropy versus magnetic interactions of magnetite grains: Experiments and application to AMS in granitic rocks, *Geophys. Res. Lett.*, *22*, 2765–2768.

Hargraves, R. B., and W. M. Young (1969), Source of stable remanent magnetism in Lambertville diabase, *Am. J. Sci.*, *267*, 1161–1177.

Hargraves, R. B., D. Johnson, and C. Y. Chan (1991), Distribution anisotropy: The cause of AMS in igneous rocks?, *Geophys. Res. Lett.*, *18*, 2765–2768.

Heller, F. (1973), Magnetic anisotropy of granitic rocks of the Bergell massif (Switzerland), *Earth Planet. Sci. Lett.*, *20*, 180–188.

Hibbard, M. (1980), Indigenous source of late-stage dikes and veins in granitic plutons, *Econ. Geol.*, *75*, 410–423.

Hrouda, F. (1982), Magnetic anisotropy of rocks and its application in geology and geophysics, *Surv. Geophys.*, *5*, 37–82.

Ishihara, S. (1977), The magnetite series and ilmenite series granitic rocks, *Min. Geol.*, *27*, 293–305.

Jackson, M. (1991), Anisotropy of magnetic remanence: A brief review of mineralogical sources, physical origins, and geological applications, and comparison with susceptibility anisotropy, *Pure Appl. Geophys.*, *136*, 1–28.

Jackson, M., W. Gruber, J. Marvin, and S. K. Banerjee (1988), Partial anhysteretic remanence and its anisotropy: Applications and grain size-dependence, *Geophys. Res. Lett.*, *15*, 440–443.

Jelinek, V. (1978), Statistical processing of anisotropy of magnetic susceptibility measures on groups of specimens, *Stud. Geophys. Geod.*, *22*, 50–62.

Jelinek, V. (1981), Characterization of the magnetic fabric of rocks, *Tectonophysics*, *79*, 63–67.

Kajitani, Y. (1977), Geology of Goyozan granitoid (in Japanese), *Magma*, *49/50*, 9–15.

Kanagawa, K. (1986), Early Cretaceous folding and cleavage in the Kitakami mountains, analysed in the Ofunato Terrane, *J. Geol. Soc. Jpn.*, *92*, 349–370.

Kano, H. (1978), Structural petrology of granite plutons (I) –The dropform plutons in the Kitakami Mountainlands, Japan (in Japanese with English abstract), *J. Mineral. Petrol. Econ. Geol.*, *73*, 97–120.

Kawano, Y., and Y. Ueda (1966), K-Ar dating on the igneous rocks in Japan (IV). Granitic rocks of the backbone range in northeastern Japan and its western district, *Sci. Rep. Tohoku Univ., Ser. 3*, *9*, 525–539.

Komazawa, M., et al. (1996), Gravity map of Kitakami district (Bouguer anomalies), *Gravity Map Ser. 7*, Geol. Surv. of Japan, Tsukuba.

Launeau, P., and A. R. Cruden (1998), Magnetic fabric acquisition mechanisms in a syenite: Results of a combined anisotropy of magnetic susceptibility and image analysis study, *J. Geophys. Res.*, *103*, 5067–5089.

Launeau, P., and P.-Y. F. Robin (1996), Fabric analysis using the intercept method, *Tectonophysics*, *267*, 91–119.

Lejeune, A.-M., and P. Richet (1995), Rheology of crystal-bearing silicate melts: An experimental study at high viscosities, *J. Geophys. Res.*, *100*, 4215–4229.

Maruyama, S., and T. Seno (1986), Orogeny and relative plate motion: Example of the Japanese islands, *Tectonophysics*, *127*, 305–329.

McCabe, C., M. Jackson, and B. B. Ellwood (1985), Magnetic anisotropy in the Treton limestone: Results of a new technique, anisotropy of anhysteretic susceptibility, *Geophys. Res. Lett.*, *12*, 333–336.

McClay, K. R. (1974), Single-domain magnetite in the Jimberlana norite, western Australia, *Earth Planet. Sci. Lett.*, *21*, 367–376.

McNulty, B. A., O. T. Tobisch, A. R. Cruden, and S. Gilder (2000), Multistage emplacement of the Mount Givens pluton, central Sierra Nevada batholith, California, *Geol. Soc. Am. Bull.*, *112*, 119–135.

Murthy, G. S., M. E. Evans, and D. I. Gough (1970), Evidence of single-domain magnetite in the Michikamau anorthosite, *Can. J. Earth Sci.*, *8*, 361–370.

Nabetani, S. (1982), Gravimetric study of the emplacement structure of Goyozan granitic pluton in the Kitakami mountainland of Japan, *Sci. Rep. Hirosaki Univ.*, *29*, 65–82.

Nabetani, S., and H. Kano (1977), Geophysical studies on plutonic structures in the Kitakami mountainland, northeastern Japan, paper presented at 7th CPPP-IGCP Meeting, Toyama, Japan.

Nakamura, N., and G. J. Borradaile (2001), Strain, anisotropy of anhysteretic remanence, and anisotropy of magnetic susceptibility in a slaty tuff, *Phys. Earth Planet. Inter.*, *125*, 85–93.

Nakamura, N., and H. Nagahama (2001), Changes in magnetic and fractal properties of fractured granites near the Nojima fault, Japan, *Island Arcs*, *10*, 486–494.

Nishioka, Y., and T. Yoshioka (2004), Geology of the Ryōri District (in Japanese with English abstract), Quadrangle Series, scale 1:50000, 49 pp., Geol. Surv. of Japan, Tsukuba.

Nye, J. F (1957), *Physical Properties of Crystals*, 322 pp., Clarendon, Oxford, U. K.

Otsuki, K. (1992), Oblique subduction, collision of microcontinents and subduction of oceanic ridge: Their implications on the Cretaceous tectonics of Japan, *Islands Arc*, *1*, 51–63.

Ozawa, K. (1984), Geology of the Miyamori ultramafic complex in the Kitakami Mountains, northeast Japan, *J. Geol. Soc. Jpn.*, *90*, 697–716.

Paterson, S. R., R. H. Vernon, and O. T. Tobish (1989), A review of criteria for the identification of magnetic and tectonic foliations in granitoids, *J. Struct. Geol.*, *11*(3), 349–363.

Picher, W. S. (1997), *The Nature and Origin of Granite*, 2nd ed., 352 pp, CRC Press, Boca Raton, Fla.

Pignotta, G. S., and K. Benn (1999), Magnetic fabric of the Barrington Passage pluton, Meguma Terrane, Nova Scotia: A two-stage fabric history of syntectonic emplacement, *Tectonophysics*, *307*, 75–92.

Renne, P. R., and T. C. Onstott (1988), Laser selective demagnetization: Application of a new technique in rock magnetism and paleomagnetism, *Science*, *242*, 1152–1155.

Renne, P. R., G. R. Scott, J. M. G. Glen, and J. M. Feinberg (2002), Oriented inclusions of magnetite in clinopyroxene: Source of stable remanent magnetization in gabbros of the Messum Complex, Namibia, *Geochem. Geophys. Geosyst.*, *3*(12), 1079, doi:10.1029/2002GC000319.

Robertson, J. K., and P. J. Wyllie (1971), Rock-water systems, with special reference to the water-deficient region, *Am. J. Sci.*, *271*, 252–277.

Rochette, P. (1987), Magnetic susceptibility of the rock matrix related to magnetic fabric studies, *J. Struct. Geol.*, *9*, 1015–1020.

Saltikov, S. A. (1958), *Stereometric Metallography*, 2nd ed., 446 pp., Metallurgizdat, Moscow.

Shibata, K., and K. Ozawa (1992), Ordovician arc ophiolite, the Hayachine and Miyamori complexes, Kitakami Mountains, northeast Japan: Isotopic ages and geochemistry, *Geochem. J.*, *26*, 85–97.

Stacey, F. D., and K. N. Wise (1967), Crystal dislocations and coercivity in fine grained magnetite, *Aust. J. Phys.*, *20*, 507–513.

Stephenson, A. (1981a), Gyromagnetic remanence and anisotropy in single-domain particles, rocks, and magnetic recording tape, *Philos. Mag. B*, *44*, 635–664.

Stephenson, A. (1981b), Gyroremanent magnetization in a weakly anisotropic rock sample, *Phys. Earth Planet. Inter.*, *44*, 635–664.

Takeuchi, M., K. Kano, M. Ujiie-Mikoshiba, and M. Komazawa (2005), Geological map of JapanIchinoseki, scale 1:200000, Geol. Surv. of Jpn., Tsukuba.

Tarling, D. H., and F. Hrouda (1993), *The Magnetic Anisotropy of Rocks*, 217 pp., CRC Press, Boca Raton, Fla.

Trindade, R. I. F., M. I. B. Raposo, M. Ernesto, and R. Siqueira (1999), Magnetic susceptibility and partial anhysteretic remanence anisotropies in the magnetite-bearing granite pluton of Tourão, NE Brazil, *Tectonophysics*, *314*, 443–468.

Trindade, R. I. F., J. L. Bouchez, O. Bolle, A. Nédélec, A. Peshler, and F. Poitrasson (2001), Secondary fabrics revealed by remanence anisotropy: Methodological study and examples from plutonic rocks, *Geophys. J. Int.*, *147*, 310–318.

Xu, W., J. W. Geissman, R. Van der Voo, and D. R. Peacor (1997), Electron microscopy of iron oxides and implications for the origin of magnetization and rock magnetic properties of Banded Series rock of the Stillwater Complex, Montana, *J. Geophys. Res.*, *102*, 12,139–12,157.

N. Nakamura, Y. Usui, and T. Yoshida, Department of Earth Sciences, Tohoku University, Sendai 980-8578, Japan. (yo_yo@dges.tohoku.ac.jp)